universität wien

MASTERARBEIT / MASTER'S THESIS

Titel der Masterarbeit / Title of the Master's Thesis

Extracellular vesicle-induced transcriptional changes in primary rat Schwann cells

verfasst von / submitted by

Julian R. Krause, B.Sc.

angestrebter akademischer Grad / in partial fulfillment of the requirements for the degree of

Master of Science (MSc)

Wien, 2023 / Vienna 2023

Studienkennzahl lt. Studienblatt / degree programme code as it appears on the student record sheet:	UA 066 834
Studienrichtung lt. Studienblatt / degree programme as it appears on the student record sheet:	Masterstudium Molekulare Biologie
Betreut von / Supervisor:	Univ.-Prof. Dr. Christine Radtke, MBA, FEBOPRAS

Acknowledgements

I want to thank my supervisor Prof. Christine Radtke for her support and for giving me the opportunity to work on this project at her laboratory. I also want to thank all the members of the group, especially Maximilian Härtinger who guided me along the way. You are a great mentor. Additionally, I want to extend my gratitude to Prof. Andreas Spittler and Günther Hofbauer (Core Facility Flow Cytometry) for helping me with the flow cytometry and the Core Facilities of the Medical University of Vienna, a member of VLSI, for their part in the sequencing experiment and initial data analysis.

Contents

Acknowledgements iii

Abstract vii

Zusammenfassung viii

1 Introduction 1

1.1 Schwann Cells in Health and Disease . . . 1

1.1.1 Nerve Injury . . . 2

1.1.2 Unsuccessful Reinnervation . . . 4

1.2 Adipose Stromal Cells . . . 5

1.3 Extracellular Vesicles . . . 5

1.3.1 Biogenesis . . . 6

1.3.2 Biological Role . . . 6

1.3.3 Therapeutic Applications of EVs . . . 7

1.4 Aim of this Thesis . . . 8

2 Methods 9

2.1 Animals . . . 9

2.2 Isolation and Culture of Primary Rat Schwann Cells . . . 9

2.2.1 Flow Cytometry . . . 9

2.3 Isolation, Culture and Differentiation of Primary Rat Adipose Stromal Cells . . . 9

2.3.1 Differentiation of Rat Adipose Stromal Cells . . . 10

2.3.2 Immunofluorescence Staining . . . 10

2.4 Enrichment and Characterization of Extracellular Vesicles . . . 10

2.4.1 Ultracentrifugation . . . 11

2.4.2 Tangential Flow Filtration/Size Exclusion Chromatography . . . 11

2.4.3 Nanoparticle Tracking Analysis . . . 11

2.4.4 EV Flow Cytometry . . . 11

2.5 Stimulation of SC with ASC-derived EVs . . . 11

2.5.1 Cell Preparation . . . 11

2.5.2 Total RNA Isolation . . . 12

2.5.3 Bulk mRNA Sequencing . . . 12

2.5.4 RNA-Seq Data Analysis . . . 12

2.5.5 RT-qPCR . . . 13

2.6 Statistical Analysis . . . 13

2.7 Nomenclature of Genes and Gene Products . . . 13

3 Results **14**
3.1 Characterization of SCs 14
3.2 Characterization of ASCs 15
3.3 Characterization of UC-enriched ASC-EVs 15
3.4 Stimulation with UC-enriched EVs does not significantly alter gene expression in SCs 16
3.4.1 Expression Patterns 17
3.4.2 Gene Clustering and Pathway Enrichment 19
3.5 Stimulation with TFF/SEC-enriched EVs shows no upregulation of key genes in SCs . 20

4 Discussion **22**

5 Conclusion and Outlook **26**

Bibliography **27**

List of Figures **36**

List of Tables **36**

Abbreviations **37**

Appendix **40**

Abstract

Extracellular vesicles (EVs) have shown potential as an alternative to cell-based therapy in nerve regeneration by enhancing proliferation of Schwann cells (SCs), promoting regeneration and improving functional outcomes. SCs are key players in nerve regeneration, enabling the remarkable regeneration seen in the peripheral nervous system (PNS) by transdifferentiating into a repair phenotype upon injury. This progression is limited by transcriptional changes following periods of denervation, resulting in loss of repair phenotype and decreasing numbers of SCs, ultimately leading to poor recovery. Overcoming these limitations presents a potential application for EVs. However, there are still too many unknowns for a safe therapeutic application. This study aimed to decipher the effects of adipose tissue-derived stromal cell (ASC) EVs on SCs at the transcriptional level. RNA sequencing of ASC-EV stimulated SCs was performed and gene expression was analyzed. This included testing for differential expression, gene clustering and pathway enrichment. SCs showed a transcriptional response to EV stimulation by activation of proliferation pathways and stimulus response pathways, but no significant differential gene expression was found. As the RNA-Seq analysis proved inconclusive, SCs were stimulated with EVs isolated by a novel enrichment method, reported to yield EVs with higher potency. Expression of selected genes was then assessed by qPCR. However, no significant upregulation of genes involved in repair phenotype or of proliferation markers was found. This highlights the need for improved potency predictors of EVs and the issues surrounding EV dosage.

Keywords: extracellular vesicles, Schwann cells, Adipose tissue-derived stromal cells, peripheral nerve regeneration, RNA sequencing, gene expression

Zusammenfassung

Extrazelluläre Vesikel (EVs) stellen eine vielversprechende Alternative zur zellbasierten Therapie in der Nervenregeneration dar, da sie die Proliferation von Schwann-Zellen (SCs) erhöhen und dadurch die Nervenregeneration fördern, sowie funktionelle Ergebnisse verbessern können. SCs nehmen nach einer Verletzung einen Reparaturphänotyp an und ermöglichen somit eine bemerkenswerte Regeneration des peripheren Nervensystems (PNS). Jedoch führt eine längere Denervierung zu Veränderungen auf transkriptioneller Ebene, die zum Verlust des Reparaturphänotyps und zu einem Rückgang der SC führen. Dadurch wird letztendlich eine erfolgreiche Regeneration verhindert. Eine mögliche Anwendung für EVs könnte darin bestehen, den Reparaturphänotyp zu verlängern. Für eine sichere therapeutische Anwendung gibt es jedoch noch zu viele unbekannte Faktoren. Das Ziel dieser Studie war es, die transkriptionellen Effekte von aus Fettgewebe isolierte Stromazell-EVs (ASC-EVs) auf SCs zu untersuchen. SCs wurden mit ASC-EVs stimuliert, anschließend erfolgte eine RNA-Sequenzierung der SCs und eine Genexpressions-Analyse. Die Analyse umfasste Tests auf differenzielle Expression, Genclustering und Pathway-Enrichment. Die SCs zeigten eine transkriptionelle Reaktion auf die EV-Stimulation durch Aktivierung von Proliferations- und Stimulusreaktionswegen. Es konnte jedoch keine signifikant differenzielle Genexpression festgestellt werden. Da die RNA-Seq-Analyse nicht eindeutig war, wurden SCs mit EVs stimuliert, die mit einer neuen Anreicherungsmethode isoliert wurden. Diese neue Methode liefert Studien zufolge EVs mit höherer biologischer Funktionalität. Die Genexpression wurde mittels RT-qPCR untersucht, es konnte aber keine signifikante Hochregulierung von Genen, die am Reparaturphänotyp beteiligt sind, oder von Proliferationsmarkern festgestellt werden. Dies hebt den Bedarf an verbesserten Wirksamkeitsvorhersagen für EVs sowie die Probleme im Zusammenhang mit der Dosierung von EVs hervor.

Keywords: Extrazelluläre Vesikel, Schwannzellen, Stromazellen aus Fettgewebe, periphere Nervenregeneration, RNA-Sequenzierung, Genexpression

1 Introduction

1.1 Schwann Cells in Health and Disease

Although the peripheral nervous system (PNS) exhibits a remarkable potential for regeneration, failure to reinnervate the target organ or tissue is common in severe peripheral nerve injury (PNI). Even after surgical reconstruction, regeneration is often limited [1]. In contrast to the central nervous system, where intrinsic capacity for regeneration is limited, the PNS has intrinsic repair mechanisms based on the transdifferentiation of SCs into a repair phenotype. However, extended periods of denervation lead to loss of the proregenerative phenotype, resulting in poor recovery. In the search for novel approaches to treat PNI, attention is turning to the molecular mechanisms that drive regeneration and the signaling involved [2].

Nerve fibers have a complex architecture, consisting of axons and their ensheathing Schwann cells arranged in fascicles and enveloped in a perineurium. The perineurium comprises layers of fibroblastic cells, forming a tough membrane that imparts elasticity and moderate resistance to stretching forces. These fascicle bundles are encased by the epineurium, a layer of connective tissue containing fibroblasts and extracellular matrix. It also includes the lymphatic and microvascular network, providing the nerve fibers with metabolic support. At the functional center of the nerve fibers are axons, myelinated processes that originate from the nerve cell soma and connect neurons to their target tissue [3].

Myelination plays a significant role in the conduction of action potentials. In unmyelinated fibers conduction of action potentials is much slower because the axonal membrane has to continuously depolarize along its entire length. Myelination of axons isolates segments of the axonal membrane, confining the depolarization of the membrane to the nodes of Ranvier. This enables saltatory conduction, which speeds up nerve impulses from 15 m/s to up to 120 m/s [3]. The glial cells responsible for myelination in the peripheral nervous system and metabolic support of axons are Schwann cells. Small axons are not myelinated and are associated with Remak SCs (RSCs), which ensheath multiple small axons in Remak bundles [4]. Axons with a diameter greater than 1-1.5 µm are myelinated by longitudinally aligned SCs that run along the axons, forming the myelin sheath [3]. SCs myelinate a defined area of axons, forming nodes of Ranvier where two myelinated segments meet. A myelin sheath forms initially as loose, uncompacted membrane wraps as the Schwann cell plasma membrane spirally winds around the axon for a few turns. The wrapping results from the entire Schwann cell following the inner (adaxonal) lip of its wrapping membrane while being anchored to the basal lamina with its outside (abaxonal) membrane. Growth of the inner membrane therefore requires disruption of the existing interaction between the prior turn of the inner membrane and the axon. Once initial wrapping has occurred, compaction is initiated through the upregulation of myelin proteins,

primarily MPZ. Despite the initiation of compaction, the myelin sheath continues to expand. The mature myelin sheath is enriched with a few key proteins, including MPZ, MBP, and PMP22, which have limited turnover and are very stable [5, 6].

1.1.1 Nerve Injury

Unlike the central nervous system (CNS), the PNS has an intrinsic capacity for regeneration after injury. There are several types of peripheral nerve injury (PNI), classified by the extent of damage to the nerve structure. The original three classes, as defined by Seddon in 1943 [7], are local demyelination with axon continuity (*neurapraxia*), the disruption of axons while leaving most of the surrounding connective tissue intact (*axonotmesis*) and, the most severe, complete nerve transection (*neurotmesis*). Sunderland built on this classification based on the severity of damage with five types of injury and this system of classification is still used in clinical practice [8]. A Type 2 or greater Sunderland nerve injury involves axonal discontinuity and Wallerian degeneration, which requires axonal regrowth [9].

If an axon is severed, sodium and calcium freely enter at the transection site, triggering uncontrolled action potentials and activating calcium-dependent proteases, which leads to degeneration of the distal axon [10]. Furthermore, retrograde transport, which acts as feedback signaling, is disrupted. This results in central chromatolysis, which is the ballooning of the neuronal cell body with disaggregation of the rough endoplasmic reticulum. To stop entry of ions at the site of injury and prevent leakage of axonal content from the proximal axon, spectrin cleavage allows the formation of membrane vacuoles that aggregate at the transection site and seal it. This permits subsequent formation of a growth cone at the axon's tip and prevents the proximal axon from undergoing degeneration [11].

The distal part of the transected axon includes its myelin sheath, which would interfere with the growth cone during regeneration. To remove the myelin and axonal debris, Wallerian degeneration is initiated (Figure 1). It starts with the fragmentation of myelin into ovoid structures that further fragment over time and are rejected by the Schwann cells, accumulating as extracellular debris. The major pro-myelin transcription factor EGR2 and the myelin-proteins MPZ, MBP, and MAG are downregulated in SCs [12, 13]. These are the initial steps of transdifferentiation for SCs into a repair phenotype. The conventional view that this represents dedifferentiation to an immature state has been challenged in recent years, with a shift toward describing the change as transdifferentiation to a repair phenotype [14, 15]. This phenotype upregulates genes associated with the developing Schwann cell, including *NCAM*, *NGFR*, and *GFAP* but also Schwann cell precursor markers as *SOX10*. The formation of the repair phenotype is dependent on the upregulation of JUN [16]. Within hours after injury, SCs begin transdifferentiation and undergo structural changes while simul-

taneously removing myelin by autophagy, termed myelinophagy, where myelin is degraded in the lysosome [17, 18]. SCs are assisted in the clearance of myelin by macrophages. Injury triggers an innate immune response in which SCs attract macrophages through cytokine secretion, primarily MCP-1 and LIF [13, 19]. After initial myelinophagy, SCs and the recruited macrophages begin to clear the remaining myelin through phagocytosis [20].

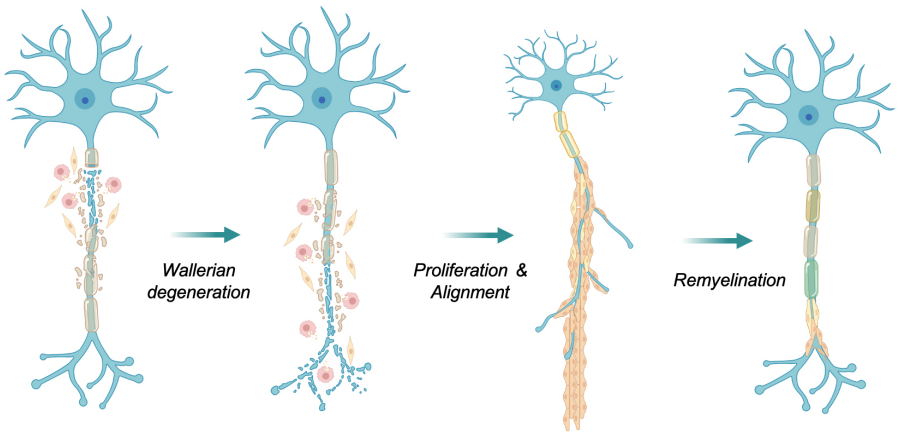

Figure 1: Nerve degeneration and regeneration. After severe injury to the axon, Wallerian degeneration begins and axonal and myelin debris is phagocytosed and cleared. Schwann cells transdifferentiate and proliferate to clear debris and to form bands of Büngner that guide the regrowing axon. After successful reinnervation, Schwann cells begin to remyelinate the axon. Figure taken with permission from Haertinger, 2023 [21].

While the distal axon dies and degenerates, the proximal axon stump continues to receive axonal components via anterograde transport. This cargo accumulates at the site of injury resulting in swelling, while also allowing for rapid formation of a growth cone using locally available material [22]. Essential for growth cone formation is the previously mentioned local rearrangement of the cytoskeleton. This rearrangement includes the depolymerization of actin, facilitating the necessary mechanical freedom to enable the plasma membrane to collapse around the sealing patch and proceed to assemble the growth cone structure. The continuing arrival of anterograde cargo and the repolymerization of cytoskeletal proteins then prompt the formation of lamellipodia and axon growth [23]. Essential for the regrowing axon is the activation of the regeneration-associated gene (RAG) program, providing energy and material for regeneration [24]. Following Wallerian degeneration, repair SCs proliferate and elongate by a factor of 2 - 3 while forming apical processes. They align longitudinally along the basal membrane, which guides the regrowing axon. These aligned SCs are known as bands of Büngner (Figure 1) [25]. The regrowing axon not only needs guidance from the aligned SCs but also heavily depends on trophic support from the SCs. The microenvironment

between SCs and axon provides molecules such as growth factors and neurotrophins to support regeneration [24]. Studies have shown JUN to be a critical factor in repair phenotype initiation [16, 26] but also in sustaining the repair phenotype [27]. Here TGFβ plays a role, as it is upregulated after nerve injury and induces Schwann cell migration and proliferation with a positive effect on re-programming and repair phenotype, thereby promoting regeneration [28]. Under optimal conditions, axonal growth continues at approximately 1 mm/d, corresponding with anterograde cargo transport in the axon, until reinnervation is achieved. Reinnervation then is the trigger for remyelination of the axon by the SCs, mediated via axonal NRG1 expression. NRG1 functions to induce redifferentiation in SCs which begin to remyelinate the regrown axon (Figure 1) [24].

1.1.2 Unsuccessful Reinnervation

Failure to reinnervate the target tissue has multiple causes. The growth cone, which forms from the proximal stump, does not simply grow as a single axon, but rather sproutes several daughter processes. These branches depend on guiding structures, ideally the endoneurial tubes of the distal nerve stump that now house repair SCs organized in bands of Büngner for growth support. An intact endoneurium can contain the axonal sprouts within and guide them directly to their target tissue. However, in cases of axonotmesis and neurotmesis, where the endoneurial tubes are transected, the regenerating axonal sprouts are not enclosed in a guiding structure anymore. To successfully reach their target tissue, they have to locate their original tubes as guiding structure or other tubes innervating the same target. Many axonal sprouts compete for a limited number of denervated fibers, and most fail to enter the distal stump and form neuromas [9, 29, 30].

To manage this, surgical reconstruction is necessary. The distal and proximal stumps should be sutured to assist in guidance of axonal regrowth. When tensionless bridging of the defect is not possible, the gold standard is the use of autografts, as they are the most suitable surrogate. But availability of autologous material is limited and its use has several drawbacks, as they sacrifice a functional sensory nerve for regeneration of a motor nerve. This can lead to sensory loss and neuroma formation at the donor site [1]. Alternatively, allografts and synthetic conduits can be used. Allografts have their own drawbacks, such as the requirement for immunosuppression. Engineered conduits are being investigated as an alternative [31], with research focusing on improving artificial conduits via integration of cells or components such as ECM molecules and neurotrophic factors or the use biomaterials such as spidersilk [32–35].

Another cause for failure of nerve regeneration is chronic denervation of the distal nerve stump. Over time, the support for growth and regeneration in the distal nerve decreases due to two factors. The repair phenotype adopted by the Schwann cells fades as JUN levels decline [27]. The number of Schwann cells also drops over prolonged periods of denervation, likely because of cell death after

loss of repair phenotype [28]. Although the reduction in cell count is only a minor contributing factor over long time periods of denervation, the loss of the repair phenotype is more critical [20]. During regeneration the regrowing axon receives neurotrophic factors from the repair Schwann cells. When the neurotrophic support is reduced, axonal regeneration is slowed and might consequently fail [24, 36]. The regenerative potential can be restored by enhancing JUN expression, making it a promising target for regulation of repair phenotype expression [27, 37].

1.2 Adipose Stromal Cells

There has been interest in the therapeutic use of stem cells for decades and various cell types have been studied [38]. Best known are mesenchymal stem cells, which in the context of *in vitro* cell culture are termed mesenchymal stromal cells (MSCs), as isolated, cultured cells are not exclusively stem cells but rather a heterogeneous mix of cells [39, 40]. They are defined by their adherence to plastic, specific antigen expression and multipotency, namely the ability to differentiate at least into adipocytes, osteocytes and chondrocytes [40]. These MSCs have been of interest for their ability to differentiate into multiple cell types and for their secretome, which provides trophic support through secretion of cytokines and other paracrine signals such as EVs [38]. There are many sources of MSCs, with adipose tissue-derived stromal cells (ASCs) being an attractive option, because ASCs are isolated from adipose tissue, which is minimally invasive and available in sufficient quantities. They are characterized in the same way as MSCs, showing the same markers and differentiation potential [38]. Therefore, ASCs have emerged as a promising cell type for regenerative therapies [41–43]. They have been shown to enhance axonal regeneration when seeded in nerve conduits [44] and when injected directly into nerve injury site [45]. But the use of stem/stromal cell-based therapies in regenerative medicine has been challenging [46], and the beneficial effects seen, have largely been attributed to paracrine signaling by various means, one of which is the release of EVs [47–49].

1.3 Extracellular Vesicles

Extracellular vesicles (EVs) are membrane-delimited microparticles of cellular origin that have a significant role in (patho-)physiological intercellular signaling [50]. They were originally described as platelet dust by Wolf and disregarded as debris until Raposo et al. showed that B lymphocytes release small EVs that are bioactive and can stimulate an adaptive immune response [51, 52]. Originally, EVs were strictly classified according to size, which was thought to equate with their biogenesis. More recently, a more continuous view that allows for overlap has emerged [53]. Small EVs are a heterogeneous mix of vesicles derived from the endolysosomal pathway called exosomes and microvesicles that form by outward budding of the plasma membrane. Exosomes are typically described as being between 30 - 200 nm in size and microvesicles as being 100 - 1000 nm in

size [50]. Even smaller in size are exomeres, which are non-membranous extracellular particles approximately 35 nm in diameter, that contain distinct functional protein and RNA cargo [54]. On the other end of the EV size spectrum are apoptotic bodies that form by blebbing of the plasma membrane during apoptosis and can be larger than 1000 nm [50].

1.3.1 Biogenesis

Small EVs have two main biogenesis pathways. Biogenesis of exosomes begins with the endosome, which is the main trafficking pathway in cells. The early endosome receives endocytosed components from several pathways, including the plasma membrane or the Golgi network. From the early endosome these components can be directly recycled for further use or they can be routed to the lysosome for degradation via the late endosome. For transport from early to late endosome/lysosome, receptors and other cargo are sorted into luminal invaginations in the early endosomal membrane with the involvement of different sorting machinery, principally ESCRT-dependent mechanisms and the bridging protein ALIX, though ESCRT-independent pathways are also described [55]. Proteins found enriched in EVs are therefore most often associated with their biogenesis, such as ESCRT components, ALIX or TSG101, but they also contain several tetraspanins, including CD9, CD63 and CD81, which can be used for characterization [56]. The cargo-enriched invaginations towards the lumen of the endosome are then pinched off and form intraluminal vesicles (ILVs). When whole regions of the early endosome detach, multivesicular bodies (MVBs) form, which traffic to the late endosome for degradation or they can be routed to the plasma membrane where they release their ILVs extracellularly as exosomes upon fusion with the plasma membrane (Figure 2) [57]. Microvesicles form by budding of the plasma membrane and direct release into the extracellular space. Cargo clusters in microdomains on the cellular side of the plasma membrane and with additional machinery form outward buds that are cargo-enriched. The biogenesis mechanisms are partly common between the endolysosomal pathway and for microvesicles but are still not completely understood in the case of microvesicles [55, 58].

1.3.2 Biological Role

Secreted by almost all cell types, small EVs can facilitate both local and systemic cell-cell communication. As EVs originate from a variety of cells and their targets are similarly varied, their mechanism of action is diverse and depends on the identity of origin and recipient cell [50]. Figure 2 illustrates that signaling can occur through either direct binding of EV surface ligands with target cell receptor, which triggers a downstream signaling cascade, or via EV intravesicular cargo. EV cargo can consist of proteins, lipids and nucleic acids, in general all the components of a vesicle and its associated molecular corona can be considered as its cargo [60, 61]. Along the biogenesis associated markers, proteins found in EVs are numerous and often include RNA-binding proteins and depend on the

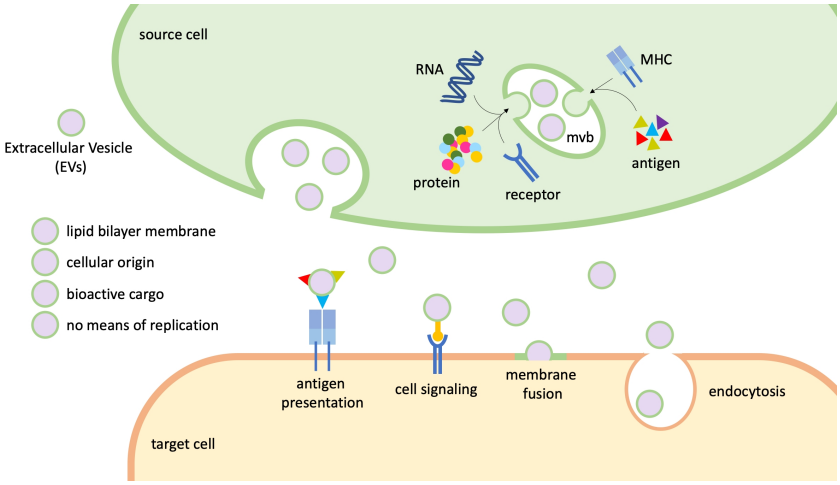

Figure 2: EV origins and signaling. Forming as ILVs from inward budding of the endosomal membrane, EVs contain various bioactive cargo, including proteins such as receptors, growth factors and antigens and nucleic acids such as microRNAs. Fusion of the MVB with the plasma membrane releases ILVs as EVs into the extracellular space. EVs act as paracrine, endocrine and autocrine messengers and can interact with their target cells in one or more of several possible ways: Immunomodulation by presenting antigens or cytokines, receptor binding and signaling, fusion and release of intraluminal cargo into target cell or endocytosis of intact particles and shuttling to lysosome. Figure taken with permission from Härtinger, 2021 [59].

subpopulation of the EVs [56, 61]. EVs primarily contain a heterogeneous selection of small RNAs with a diverse set of functions, including regulation of gene and protein expression in the target cells [62, 63]. In general, the binding of EVs to their target is mediated by specific interaction of proteins on the EV surface and membrane receptors of the target cell, these include tetraspanins, integrins and ICAMs as well as proteoglycans and even ECM components. Depending on the EVs fate, this binding can trigger signaling pathways in the recipient cell directly or mediate internalization via endocytosis or macropinocytosis. When internalized, they eventually end up in the lysosome via the endolysosomal pathway, where they are degraded. Cargo can potentially avoid degradation and escape from lysosomes, which is being investigated [58, 64]. The range of functional responses that EVs can induce through binding is varied. First described by Raposo et al., B-lymphocyte EVs were found to be able to induce an antigen response in T cells [52]. Since then, numerous functional responses have been described, not only induced by EV binding, but also by cargo delivered through EV internalization [55].

1.3.3 Therapeutic Applications of EVs

EVs have the advantage of lower immunogenicity while avoiding the major problem of engraftment of viable replicating cells. Therefore, the use of stem/stromal cell-derived EVs is being investigated for

many applications [48, 65, 66] and similar therapeutic effects have been observed with stem/stromal cell-derived EVs compared to stem cell therapy itself [67, 68]. In PNI, EVs have been shown to promote regeneration and improve functional recovery [69]. Mesenchymal stromal cell-derived EVs have been shown to induce neurite outgrowth [70] and adipose stromal cell-derived EVs have been shown to promote proliferation of SCs among others [71–74]. These promising results are countered by too many unknowns [58]. The exact mode of action remains elusive [68] and questions about potency and functionality of EV preparations remain unanswered [75, 76].

1.4 Aim of this Thesis

EVs have been investigated as an alternative to cell-based therapies in nerve regeneration owing to their paracrine signaling functions and comparable efficacy. EVs could potentially assist nerve regeneration by prolonging the repair phenotype or enhancing proliferation, though they might not replace surgery completely but aid in regeneration alongside it. Recent studies suggest that EVs derived from MSCs or ASCs promote axonal outgrowth and regeneration and support SC proliferation [77]. Identifying the molecular mechanisms underlying these proregenerative effects could lead to novel therapeutic strategies. This study aims to investigate the transcriptional effects of rASC-EVs stimulation in rSC. While detailed transcriptional data exists for the injured nerve and SCs in the repair phenotype, as well as data for the developing SC precursors [13, 78, 79], expression data for EV-treated SCs is limited [74]. Such data is critical in understanding the mode of action of EVs in target cells on the path to a therapeutic application of EVs.

2 Methods

2.1 Animals

Sciatic nerve tissue and adipose tissue was harvested from young adult male Lewis rats. Animals were sacrificed in accordance with the “Bundesgesetz über Versuche an lebenden Tieren [Federal Act on Experiments on Live Animals]” (TVG 2012, §2, 1) and the “Directive 2010/63/EU of the European Parliament and of the Council on the protection of animals used for scientific purposes.”

2.2 Isolation and Culture of Primary Rat Schwann Cells

Isolation and culture was performed as previously described [32, 71, 82]. In brief, sciatic nerve tissue was cut into 1.5 cm long pieces and fascicles were pulled out of the epineurium using tweezers. Fascicles were digested overnight in digest solution containing 0.125 % collagenase Type IV (GIBCO), 1.25 U/ml Dispase II (SIGMA) and 3 mM CaCl. The next day tissue was resuspended and centrifuged at 300×g for 5 min at RT. Cells were resuspended in SC expansion medium (SCEM) consisting of MEMα (GIBCO) supplemented with 1 % P/S, 1 mM sodium pyruvate, 25 mM HEPES, 10 ng/ml hFGF basic, 10 ng/ml hHeregulin-beta 1.5 ng/ml huPDGF-AA (all PeproTech), 0.5 % N2 supplement (GIBCO), 2 mM forskolin (SIGMA) and 2 % FCS and added to PLL/laminin-coated 6-well plates.

After reaching 90 % confluency, SCs were enriched using the differential adhesion properties of SC and contaminating cells and subcultured. Cold Accutase was added for 7 to 10 min and cell detachment was checked under the microscope. Cells were centrifuged at 300×g for 5 min, resuspended in αMEM+ (SCEM not supplemented with growth factors) and seeded in uncoated culture flasks. After 30-40 min of incubation at 37 ℃ the supernatant containing SCs was collected and centrifuged at 300×g for 5 min. SCs were then resuspended in SCEM and seeded in coated wells.

2.2.1 Flow Cytometry

Single-cell suspension of SCs was labeled with fluorophore-conjugated antibodies and DAPI was added prior to analysis as live/dead stain for 10 min. Antibodies are listed in supplemental Table S1. Following staining cells were washed (300×g for 5 min) and measured on a CytoFLEX LX (Beckman Coulter, Brea, CA, USA). Data was analyzed using FlowJo v10.8.1 software (FlowJo LLC, Ashland, OR, USA).

2.3 Isolation, Culture and Differentiation of Primary Rat Adipose Stromal Cells

Intra-abdominal, perirenal and -gonadal adipose tissue was washed with HBSS supplemented with 1 % Pen/Strep. Connective tissue and blood vessels were manually removed, adipose tissue was minced and digested with 0.5 mg/ml Collagenase I in HBSS for 20-30 min at 37 ℃ while agitating every 5 min. Digested adipose tissue was then centrifuged at 1000×g for 10 min. Pellet was washed

with HBSS + 0.5 % BSA followed by centrifugation at 500×g for 5 min. Subsequently, pellet was resuspended in growth medium and seeded. Growth medium was changed every 2 - 3 d. Cells were subcultured at 50 to 60 % confluency up to passage 5.

2.3.1 Differentiation of Rat Adipose Stromal Cells

Multipotency of rat adipose stromal cells was verified using a Rat Mesenchymal Stem Cell Functional Identification kit (R&D systems, Minneapolis, MN, USA) according to the manufacturer's instructions. For each differentiation cells were cultured for 21 days in respective lineage differentiation media. After 21 days cells were fixed using 4.5 % paraformaldehyde (PFA). Adipogenic differentiation was demonstrated by immunofluorescence (IF) staining using anti-mFABP4 antibody and lipid droplets were visualized with oil red O. Osteogenic differentiation was confirmed by anti-hOsteocalcin IF-staining and Alizarin Red stain.

2.3.2 Immunofluorescence Staining

To allow intracellular immunofluorescence staining and to prevent non-specific antibody binding, cell membranes were permeabilized and non-specific binding blocked by incubation of fixed cells in PBS supplemented with 10 % swine serum, 1 % BSA and 0.3 % Triton X-100 for 20 min. Antibodies used are listed in supplemental Table S1. Cells were incubated with primary antibody overnight at 4 ℃ diluted in PBS supplemented with 10 % swine serum, 1 % BSA and 0.03 % Triton X-100. Cells were washed 3 times with PBS and secondary antibody was incubated for 2 h at RT in PBS supplemented with 10 % swine serum, 1 % BSA and 0.03 % Triton X-100. Cells were then washed 3 times in PBS, incubated with 1 µg/µL DAPI for 10 min and washed again 3 times in PBS. Images were acquired on a Zeiss LSM 980 with AiryScan 2 (Carl Zeiss Microscopy, Oberkochen, Germany) using a 20x dry objective. Images are presented as maximum intensity projection of 3D airyscan processed Z-stacks acquired at Nyquist optimum distance. Processing was performed in the Zeiss ZEN 3.8 software (Carl Zeiss Microscopy).

2.4 Enrichment and Characterization of Extracellular Vesicles

At 60-80 % confluency ASC cultures were washed twice with PBS and incubated with serum-free culture medium for 24 h. Conditioned culture medium was subjected to successive centrifugations at 300×g for 10 min and 2,000×g for 20 min to remove cells. Cell-free supernatant was then centrifuged at 20,000×g for 20 min to remove debris and filtered using a 0.22 µm PVDF syringe filter. This was followed by Ultracentrifugation (UC) or Tangential Flow Filtration/Size Exclusion Chromatography (TFF/SEC).

2.4.1 Ultracentrifugation

Filtered supernatant was ultracentrifuged using a T-865 fixed angle rotor (Thermo Fisher Scientific, Waltham, MA, USA) at 100,000×g for 90 min to pellet EVs. Supernatant was discarded and EVs were resuspended in PBS. Two resuspended pellets were pooled and ultracentrifuged at 100,000×g for 90 min and resuspended in 100 µL of PBS.

2.4.2 Tangential Flow Filtration/Size Exclusion Chromatography

Conditioned medium was obtained as described above and loaded into a TFF EVs Small cartridge (HansaBioMed LS, Tallinn, Estonia). 40 mL of conditioned medium were filtered consecutively and retentate was then washed with PBS and recovered. TFF filtered sample was then loaded on a qEV1 70 nm SEC column (IZON Science, Christchurch, New Zealand) and 1 fraction was collected using an automatic fraction collector (IZON Science) with a buffer volume of 4.0 mL and a fraction volume of 2.8 mL.

2.4.3 Nanoparticle Tracking Analysis

Size distribution and concentration of EVs was measured using a ZetaView PMX-120 (Particle Metrix, Inning am Ammersee, Germany). Device was calibrated with 100 nm beads diluted 1:250,000. Devices settings were sensitivity 80, shutter 100 and frame rate 30. 11 positions were recorded in 3 cycles. Maximum area was set to 1000, minimum area to 10, minimum brightness to 30 and tracelength to 15. Temperature control was set to 25 ℃.

2.4.4 EV Flow Cytometry

UC-enriched EVs were incubated with primary antibodies for 2 h. Antibodies are listed in supplemental Table S1. For the last 30 min of incubation CMG was added at a 1:1000 dilution. After incubation final volume was adjusted with PBS to achieve a 1:5 EV dilution. Measurements were performed on a CytoFLEX LX with B525-FITC as trigger channel. Threshold was set so measurement of PBS resulted in less than 1000 particles over 120 sec. Accordingly, primary threshold channel was set to B525-FITC at 660. After 30 sec of equilibration, samples were measured on slow flow rate (10 µL/min) for 120 sec. Data were analyzed using FlowJo software.

2.5 Stimulation of SC with ASC-derived EVs

2.5.1 Cell Preparation

For subsequent RNA sequencing SCs were seeded at a density of 18,000 cells/cm^2 or 9,000 cells/cm^2 for +24 h and +72 h time points respectively. After 24 h UC-enriched EVs were added to the SCs at a relative concentration of 5,000 particles/cell as measured by NTA and incubated for 24 h and 72 h respectively. For qPCR SCs were seeded at a density of 10,000 cells/cm^2 and TFF/SEC-enriched

EVs were added after 24 h and incubated for 72 h. SCs were stimulated with 20,000 particles/cell of TFF/SEC-enriched EVs. Stimulation for RNA-seq was performed in five biological replicates (n=5) and for qPCR in six biological replicates (n=6). SC cultures of the same donors without addition of EVs served as control.

2.5.2 Total RNA Isolation

Total RNA was isolated using a RNeasy Mini kit (QIAGEN, Venlo, Netherlands) according to the manufacturer's instructions. After isolation, RNA concentration was measured using a NanoDrop One Spectrophotometer (Thermo Fisher Scientific).

2.5.3 Bulk mRNA Sequencing

mRNA sequencing by poly (A) capture was performed by the Core Facilities of the Medical University of Vienna, a member of VLSI. Sequencing libraries from total RNA of the samples were prepared using the NEBNext Single cell / LowInput RNA Library Prep Kit (E6420) according to manufacturer's instructions. Libraries were QC checked on a Bioanalyzer 2100 (Agilent) using a High Sensitivity DNA Kit for correct insert size and quantified using Qubit dsDNA HS Assay (Invitrogen). Pooled libraries were sequenced on a NextSeq500 instrument (Illumina) in 1x75bp single-end sequencing mode. On average, 24 million reads per sample were generated. Reads in fastq format were generated using the Illumina bcl2fastq command line tool (v2.19.1.403). Reads in fastq format were aligned to the rat reference genome version rnor 6.0 (downloaded from ensembl 2019-05-28) with ensembl 96 annotations (downloaded from ensembl 2019-05-28) [83] using STAR aligner [84] version 2.6.1a in 2-pass mode. Raw reads per gene were counted by STAR. Differential gene expression was calculated using DESeq2 [85] version 1.22.2. Transcripts per million (TPM) were generated by RSEM [86].

2.5.4 RNA-Seq Data Analysis

Analysis of RNA sequencing data was performed by Core Facility Bioinformatics, Medical University of Vienna. Further analysis was performed using iDEP [87] and DESeq2. Principal component analysis (PCA), heatmap generation and k-means clustering were performed in the iDEP environment. PCA was set to first two components on x- and y-axis. Heatmap was generated using correlation for distance and average as linkage, with a cut-off Z score of 4. Only selected genes of interest were used as input for heatmap with no ranking of most variable by standard deviation. k-Means clustering was performed on 500 most variable genes based on standard deviation with 4 clusters as output. Per gene normalization was set to mean center and GO Biological Process was the pathway database used for enrichment. DESeq2 was used for differential gene expression analysis. The false discovery rate (FDR) cut-off was set to 0.05 and the minimum fold change to 2.

2.5.5 RT-qPCR

cDNA was synthesized with LunaScript RT SuperMix (New England Biolabs, Ipswich, MA, USA), using 50 ng of RNA per sample. qPCR was performed using Luna Universal qPCR Master Mix (New England Biolabs) on a 7500 fast system (Applied Biosystems, Waltham, MA, USA) using commercially available primers (SIGMA) listed in supplemental Table S2. Expression was calculated as $\Delta\Delta$CT normalized on ACTB and GAPDH housekeeping genes without primer efficiency correction. Replicate values of both housekeeping genes for each sample were averaged by geometric mean and subtracted from averaged sample cycle threshold (CT) value for ΔCT. ΔCT of EV treated sample was then subtracted from ΔCT of control sample for each donor and gene for $\Delta\Delta$CT. Log2 fold change was then calculated from $\Delta\Delta$CT.

2.6 Statistical Analysis

Data were analyzed using GraphPad Prism 9.5.0 software (GraphPad Software, Boston, MA, USA) and are presented as mean $\pm$ standard deviation (SD). Size of EVs is given as median. Where applicable, replicate values were averaged and normalized to untreated control. For analysis of differentially expressed genes an adjusted p-value cutoff (FDR) of 0.05 was used.

2.7 Nomenclature of Genes and Gene Products

As this study was performed using primary rat cells, the following chapters will adhere to the gene and protein nomenclature defined by the International Committee on Standardized Genetic Nomenclature for Mice and the Rat Genome and Nomenclature Committee [88–90].

3 Results

3.1 Characterization of SCs

SCs were isolated from from sciatic nerve fascicles and cultured in PLL/laminin-coated culture dishes and exhibited phenotypical spindle morphology and alignment from p2 onward (Figure 3A). SCs were characterized by flow cytometry using the antigen markers CD271, CD11bc, CD90.1 and O4. Representative plots are shown (Figure 3C). SCs were consistently positive for NGFR at almost 100 % and negative for microglia, monocyte and fibroblast markers. O4 expression was inconsistent with donor variability ranging from 2 % to 80 % and a mean of 45 % (Figure 3B).

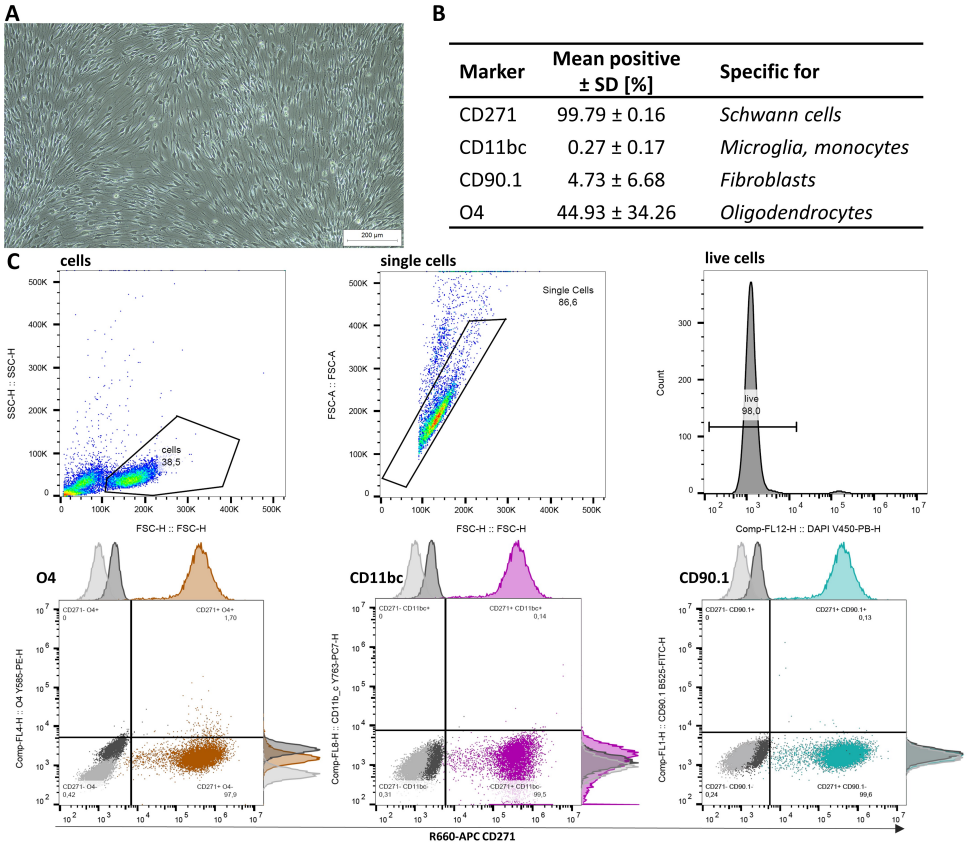

Figure 3: Characterization of SCs by flow cytometry. (**A**) SCs in p2 showed phenotypical spindle morphology and alignment in phase contrast images. (**B**) Population statistics for SCs with markers and their targets showed almost all cells were positive for NGFR with low positivity for contaminating cell markers, demonstrating SC character of cells. Mean of 6 donors. (**C**) Flow cytometric analysis of marker expression with gating strategy shown. Scatter plot of recorded events with cells gated (cells). Singlets gated on cells (single cells). Live cells gated by DAPI negative signal of singlets (live cells). Marker expression was analyzed on events considered live single cells, comparing CD271 expression vs O4, CD11bc and CD90.1 expression. Light gray shows unstained cells and dark gray shows cells stained with isotype control. n=6 with representative donor shown.

3.2 Characterization of ASCs

ASC were isolated from intra-abdominal adipose tissue and expanded to source EVs. ASC showed a characteristic morphology in phase contrast (Figure 4A1) and were plastic adherent. Multilineage potential was verified by differentiation and staining. Adipogenic differentiation was confirmed by oil red O staining of lipid vacuoles (Figure 4A2) and by IF staining for mFABP4 (Figure 4B). Osteogenic differentiation was confirmed by positive Alizarin red stain for calcium deposits (Figure 4A3) and by IF staining for hOsteocalcin (Figure 4C).

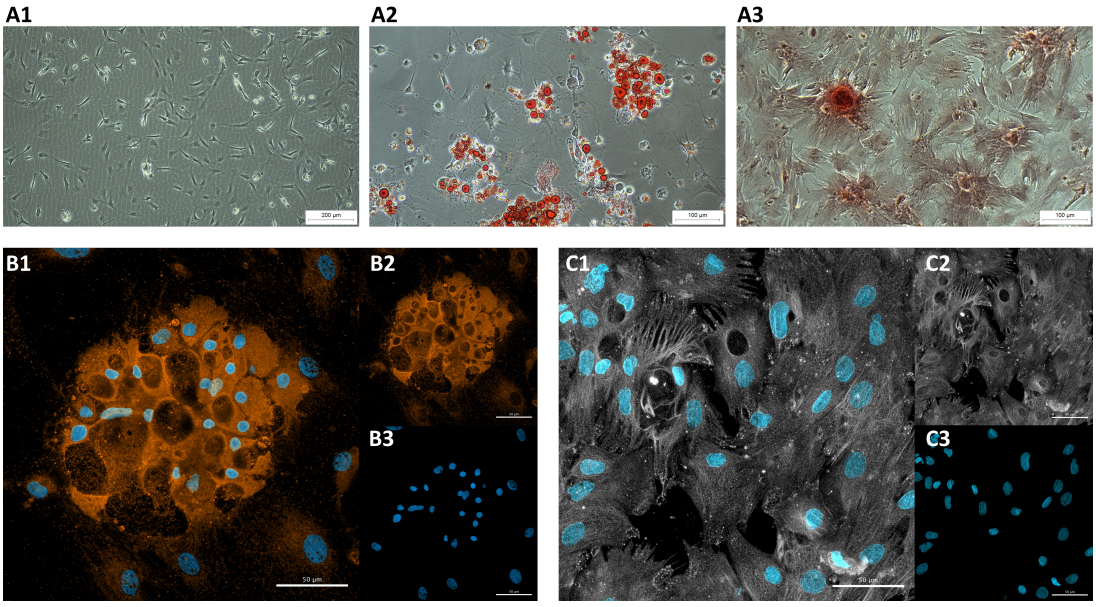

Figure 4: Differentiation of ASCs into adipocytes and osteocytes demonstrates multilineage potential. (**A**) Undifferentiated rASCs in p3 showed characteristic morphology in phase contrast images (A1). Adipogenic differentiation shown by staining of lipid droplets using oil red O staining (A2). Osteogenic differentiation shown by positive alizarin red stain (A3). (**B**) and (**C**) Differentiation shown by immunofluorescence staining. Adipogenic differentiation shown by immunofluorescence staining for mFABP4 (B2), DAPI (B3) and merged channels (B1). (**C**) Osteogenic differentiation shown by immunofluorescence staining for hOsteocalcin (C2), DAPI (C3) and merged channels (C1). Scale bars in (B) and (C) equivalent to 50 µm.

3.3 Characterization of UC-enriched ASC-EVs

EVs were enriched by differential ultracentrifugation after 24 h of serum-free conditioning. Size distribution (Figure 5A1) and concentration (Figure 5A2) were measured by NTA at 109 nm median size and a mean concentration of 9.95×10^8 particles/mL for three independent EV preparations (Figure 5A2). Presence of tetraspanins CD9, CD63 and CD81 and the absence of cytochrome C in the preparations was demonstrated by flow cytometry (Figure 5B).

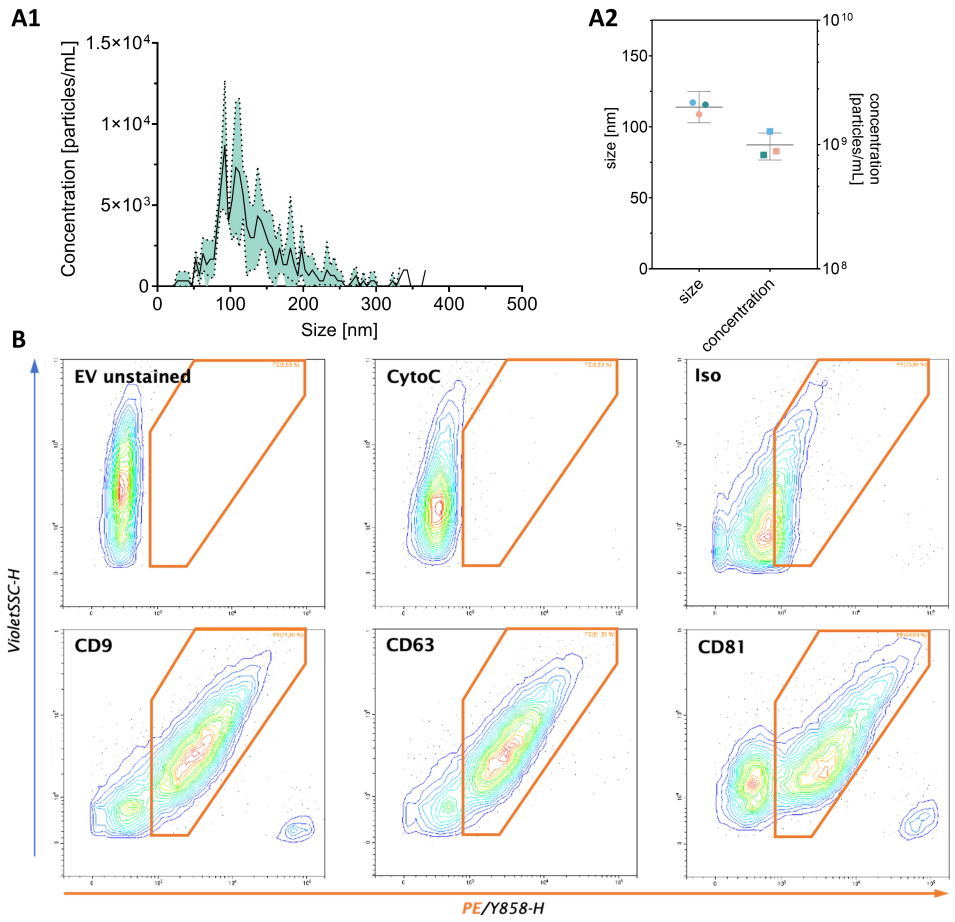

Figure 5: Characterization of UC-enriched EVs. (**A**) Size and concentration measured by NTA shows defined median size of particles with irregular size distribution in three EV preparations (A1). Total concentration and mean size of EV preparations (A2). n=3, mean with SD. (**B**) Flow cytometric characterization demonstrated EVs positive for tetraspanins. CMG stained EV preparations were measured by flow cytometry triggering on B525-FITC channel. Non-AB-stained EVs were used to define PE^+ gate (EV unstained). Anti-Cytochrome C and isotype stain served as negative control (CytoC + Iso). Tetraspanin positive EVs (CD9, CD63, CD81).

3.4 Stimulation with UC-enriched EVs does not significantly alter gene expression in SCs

SCs were treated with UC-enriched EVs at a ratio of 5,000 particles/cell to investigate time-dependent transcriptional changes mediated by EVs. After 24 h and 72 h, total RNA was isolated and mRNA sequenced. Principal component analysis was performed to observe sample grouping (Figure 6A) and samples grouped along the first two dimensions of PCA consistent with time and treatment variables. Overlap between EV-treated and control groups was more pronounced for samples from the 72 h time point.

RNA-seq analysis identified a total of 985 differentially expressed genes in all comparisons (Figure 6B). Of these, only four were found between EV and control at the same time point, all were

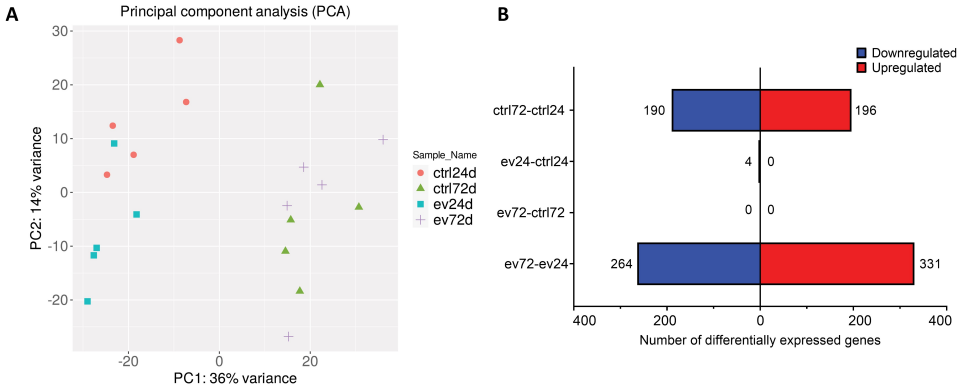

Figure 6: PCA plot of RNA-seq data and number of differentially expressed genes. (**A**) Visual representation of first two principal components of gene expression data showed sample grouping along time and treatment variables. Samples colored by treatment and time point. (**B**) DESeq2 identified 985 differentially expressed genes in all comparisons, with only four genes in comparisons between treatment and control at the same time point. FDR cut-off was set to 0.05 and minimum fold change to 2.

downregulated. All other differentially expressed genes were found in comparisons between time points, i.e. control at 72 h vs control at 24 h. The four genes downregulated after 24 h of EV stimulation were *Tet3*, *Mypop*, *Il4r* and *Atp13a2*. *Tet3* has a role in DNA demethylation and transcriptional regulation, *Mypop* acts as a transcriptional repressor, *Il4R* encodes for the IL4 receptor for both interleukin 4 and interleukin 13 and is canonically involved in the inflammatory response of lymphocytes. *Atp13a2* encodes for an ATPase required for lysosomal and mitochondrial maintenance. *Mypop* and *Il4r* were also found in comparison between EV-treated SCs at 72 h vs 24 h, where they were upregulated. As not enough differentially expressed genes were found in comparisons between EV and control at the same time point, no further analysis with differentially expressed genes was performed.

3.4.1 Expression Patterns

To investigate whether EVs have an influence on the repair phenotype and the regenerative potential of SCs, 24 genes of interest were selected and plotted as a heatmap (Figure 7). Genes encoding for myelin proteins such as *Mpz*, *Mbp*, *Pmp22*, *Mag* and *Plp1* as well as the major pro-myelin transcription factor *Egr2* appeared to be upregulated after 72 h independent of EV treatment, with *Mag* showing donor variability. In addition, the differentiation markers *S100b* and *Gfap* showed slight upregulation after 72 h, while Schwann cell precursor marker *Sox10* appeared to have relatively constant expression. Macrophage-associated antigen *Cd68* and fibroblast marker and ECM component *Col1a1* again showed a slight downregulation at 72 h with no correlation to EV treatment.

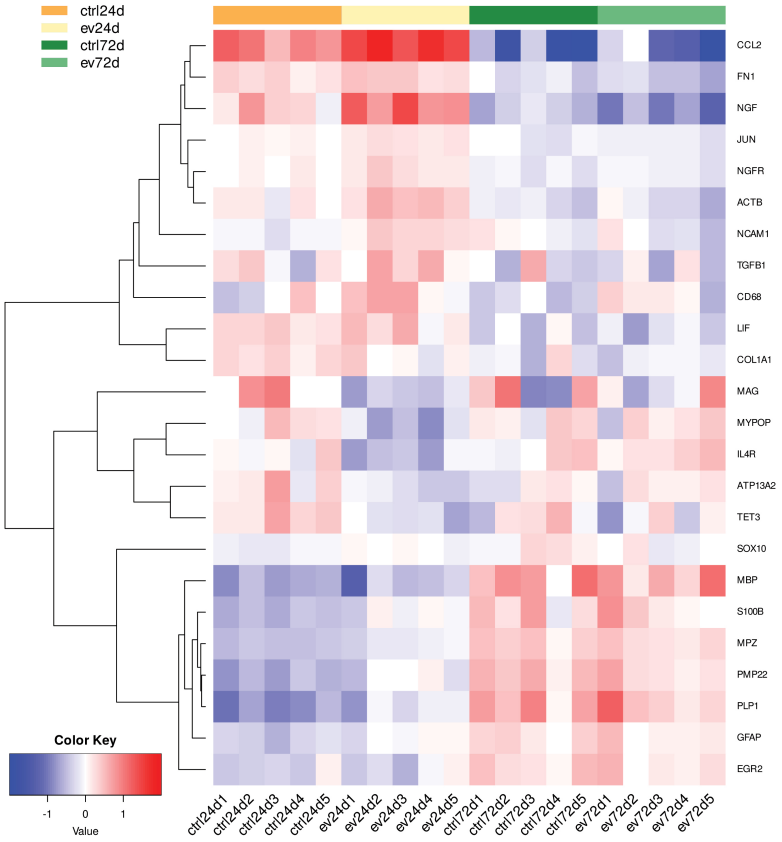

Figure 7: Heatmap showing expression pattern of 24 genes of interest. Experimental conditions grouped on Y-axis. Clustering was performed using correlation as distance measure, cut-off Z-score was set to 4 and linkage set to average.

The differentially expressed genes *Tet3*, *Mypop*, *Il4r* and *Atp13a2* did not show an expression pattern correlating with treatment or time in the heatmap representation. Macrophage attractant *Lif* showed slight downregulation after 72 h while *Ccl2* (*MCP-1* in humans) showed strong upregulation with EV treatment after 24 h and strong downregulation after 72 h in both EV-treated and control group. The ECM and migration gene regulator *Fn1* also showed slight downregulation after 72 h. Repair phenotype associated genes *Ncam1*, *Ngfr* and *Jun* were only slightly regulated without clear pattern. *Ngf* showed upregulation with EV treatment after 24 h and downregulation after 72 h in both groups but stronger with EV treatment. Housekeeping gene *Actb* was not strongly regulated but showing slightly upregulated expression at 24 h with EV treatment. *Tgfb1* regulates cell proliferation, differentiation and growth and did not show a clear expression pattern. Genes *Fgf8* and *Gapdh* were not found in RNA-seq data set. Overall for most genes inter-donor variability was stronger than response to EV treatment. For 10 genes, including genes responsible for myelination, a change in expression could be seen from 24 h to 72 h. Only *Ccl2* and *Ngf* showed a discernible response to EV treatment, with upregulated expression at 24 h and downregulation at 72 h compared to control.

3.4.2 Gene Clustering and Pathway Enrichment

To further analyze non-differentially expressed genes, k-means clustering was performed on the 500 most variable genes, resulting in four clusters. Cluster A contained 161 genes upregulated at 24 h and downregulated at 72 h. Cluster B contained 180 genes that were downregulated at 24 h and upregulated at 72 h. Cluster C contained 66 genes, that showed relatively consistent expression for all conditions or time points but varied between donors. The clusters were then subjected to GO Biological Process enrichment analysis. The enriched pathways and their size in terms of number of genes are shown in Table 1. Pathways related to Schwann cell, nervous system function and responses to EV stimulation were highlighted. In cluster A, with genes upregulated at 24 h and downregulated at 72 h, these included pathways such as axon ensheathment, myelination and regulation of glial cell differentiation.

Table 1: Enriched pathways of 500 most variable genes. (**Cluster A**) Enriched pathways for genes upregulated at 24 h and downregulated at 72 h. Cluster contained 161 genes. (**Cluster B**) Enriched pathways for genes downregulated at 24 h and upregulated at 72 h. Cluster contained 180 genes. (**Cluster C**) Enriched pathways for genes showing same regulation in genes at all conditions and time points for same donor but varying between donors. Cluster contained 66 genes. K-means clustering of 500 most variable genes with 4 clusters. 4^{th} cluster without enriched pathways excluded. Number of total genes in each pathway shown under Genes. GO Biological Process pathway database was used for enrichment analysis.

Genes	Cluster A	Genes	Cluster B
10	Oligodendrocyte differentiation	69	Response to chemical
12	**Glial cell differentiation**	41	Regulation of cell population proliferation
27	System process	58	Response to organic substance
13	**Gliogenesis**	43	**Cell population proliferation**
9	**Ensheathment of neurons**	37	Response to endogenous stimulus
9	**Axon ensheathment**	27	Response to organic cyclic compound
58	System development	54	Cellular response to chemical stimulus
36	**Nervous system development**	33	System process
59	Multicellular organism development	47	**Cell surface receptor signaling pathway**
3	Spermine metabolic process	32	**Cellular response to endogenous stimulus**
8	**Myelination**	30	Cell adhesion
6	**Regulation of glial cell differentiation**	30	Biological adhesion
5	Regulation of oligodendrocyte differentiation	47	Regulation of multicellular organismal process
17	**Nervous system process**	33	**Cell migration**
13	**Regulation of nervous system development**	29	Tube development

Genes	Cluster C
21	Anatomical structure formation involved in morphogenesis
29	Anatomical structure morphogenesis
14	Angiogenesis
21	**Cell migration**
13	Ameboidal-type cell migration
23	Tissue development
21	**Cell motility**
21	Localization of cell
15	Blood vessel development
14	Blood vessel morphogenesis
26	Regulation of multicellular organismal process
11	**Tissue migration**
18	Circulatory system development
15	Vasculature development
16	Tube morphogenesis

Cluster B with genes downregulated at 24 h and upregulated at 72 h had enriched pathways such as cell population proliferation, cellular response to endogenous stimulus and cell migration. Cluster C with time and condition independent but donor variable expression showed enriched pathways such as cell migration, cell motility and tissue migration.

3.5 Stimulation with TFF/SEC-enriched EVs shows no upregulation of key genes in SCs

The combination of tangential flow filtration and size exclusion chromatography as enrichment and purification methods for EV preparation has been reported to yield EVs with more biological function than ultracentrifugation-based methods [60]. Since RNA-seq analysis showed inconclusive results with UC-enriched EVs, TFF/SEC was used as an alternative enrichment method. TFF/SEC-enriched EVs were larger than UC-enriched EVs as measured by NTA at 136 nm median size (Figure 8).

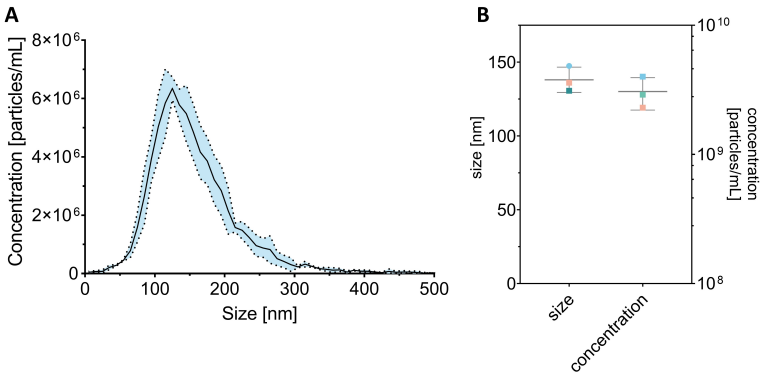

Figure 8: Characterization of TFF/SEC enriched EVs by NTA. (**A**) Size distribution of three EV preparations showed uniform size. (**B**) Total concentration and mean size of EV preparations. n=3, mean with SD

Concentration was measured at 3.07×10^9 particles/mL. This increased size may be attributed to membrane proteins present on TFF/SEC-enriched EVs that are removed by ultracentrifugation.

SCs were stimulated with TFF/SEC-EVs at a ratio of 20,000 particles/cell to investigate bioactive function of EVs enriched by TFF/SEC via transcriptional changes in SCs. qPCR was used to quantify expression of genes responsible for repair phenotype, neuron support and proliferation markers (Figure 9). Gene expression was normalized to geometric mean of housekeeping genes *Actb* and *Gpadh*. Expression of EV-treated samples was then normalized to control as log2fold change.

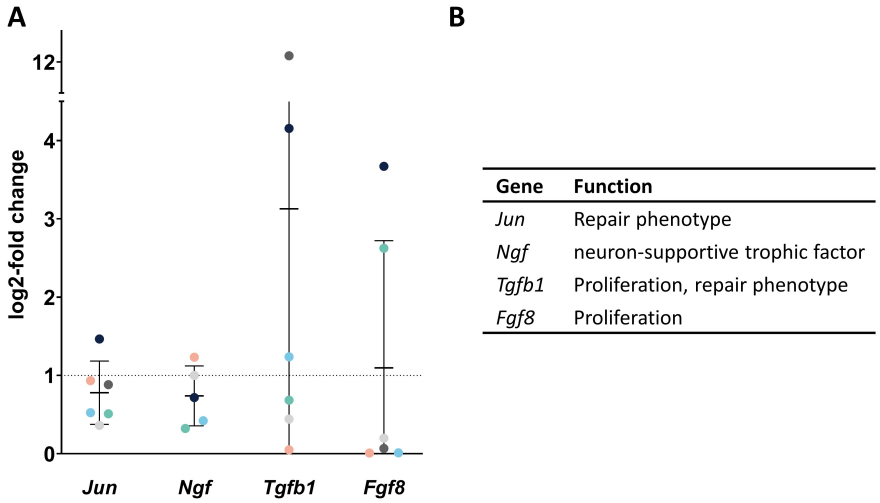

Gene	Function
Jun	Repair phenotype
Ngf	neuron-supportive trophic factor
Tgfb1	Proliferation, repair phenotype
Fgf8	Proliferation

Figure 9: Relative gene expression measured by qPCR. (**A**) Log2-fold change in gene expression of EV-treated samples normalized to expression levels of control group. Samples colored by donor. Outliers were identified by ROUT method with FDR set to 0.01, resulting in 1 outlier removed from NGF. (**B**) Genes and their function.

Jun and *Ngf* grouped closely and showed reduced expression relative to control stimulated with vehicle only, with two donors showing slightly increased expression. *Tgfb1* and *Fgf8*, a growth factor involved in cell proliferation, differentiation and migration, showed a large range with some EV treated donors grouping with lowered expression and others showing strongly increased expression. These results show inconclusive effects of EVs on SCs with large donor variance. Overall, transcriptional changes can be observed from EV treatment but they are either not significant or have a large variance.

4 Discussion

In this study, primary rat SCs were stimulated with ASC-derived EVs and their mRNA was sequenced 24 h and 72 h post-stimulation. To ensure cell identity, flow cytometry was performed using CD271 as a marker for SCs and CD90.1 and CD11bc as markers for contaminating fibroblasts and macrophages respectively. Characterizing the SCs was essential as sequencing results could be biased by contaminating cells that could have responded differently to EV stimulation. Characterization showed cell population was almost 100 % positive for CD271, under 5 % positive for CD90.1 and less than 1 % positive for CD11bc, which established that cells had SC character. The glycosphingolipid galactocerebroside O4 is described as an oligodendrocyte marker [91], but it has also been found to be expressed by SCs in both myelinating and non-myelinating cells [92, 93]. Levels of O4-positive SCs varied between donors, suggesting the presence of subpopulations, as shown by flow cytometric characterization. In culture, SCs displayed phenotypical spindle morphology and alignment. To confirm the stromal characteristics of ASCs, their multilineage potential was demonstrated. However, in order to meet the minimal criteria for multipotent mesenchymal stromal cells, expression of markers CD105, CD73 and CD90 and absence of markers CD45, CD31 and CD11bc would have to be confirmed as well [40]. This is based on the variety of isolation methods and tissues from which MSCs can be isolated and the need to compare results from these cells. The identifying criteria allow for results from studies using MSCs to be compared and contrasted while ensuring cells are sufficiently similar. EVs enriched through UC were characterized by size and concentration analysis showing an irregular size distribution with a median size of 109 nm. The presence of tetraspanin markers was confirmed by flow cytometry.

PCA was employed as an initial quality control check of RNA-seq data. It reduces and projects differences in all gene expression levels for each donor onto two axes, hence allowing for observation of trends in expression data and is expected to show grouping along the variables of the experiment. PCA of RNA-seq data showed donors grouped based on time and treatment, validating the experimental setup was discernible in the data. DESeq2 analysis identified only four genes as differentially expressed at 24 h and none at 72 h between treatment and control. The genes *Tet3*, *Mypop*, *Il4r* and *Atp13a2* were significantly downregulated in the comparison between EV-treated SCs and the control group. None of these genes are typically associated with nerve injury or regeneration and no clear correlation to the repair phenotype can be established. The injured sciatic nerve atlas (iSNAT) provides a single-cell RNA-sequencing analysis of both naïve and crushed mouse sciatic nerves at 1, 3 and 7 days post-injury [78]. This dataset shows that *Tet3* expression is low in SCs in the naïve mouse nerve and remains relatively unchanged after crush injury. In the naïve nerve, baseline *Mypop* expression is also low and decreases after injury with a slight recovery at 7 d, this trend is mirrored by *Atp13a2*. *Il4r* shows low expression in SCs in the naïve nerve and strong upregulation

after 24 h. At 3 d post-injury, expression returns to baseline and remains there. Upregulation of *Il4r* in SCs 24 h after crush injury may be related to the innate immune response elicited by injury and the recruitment and infiltration of macrophages and other immune cells into the injured nerve. Direct comparison between the data collected in this study from cultured rat SCs stimulated with EVs and the iSNAT data collected from mice before and after crush injury is not reasonable. However, it suggests that, apart for *Il4r*, the genes expressed differentially in this study are not strongly regulated in response to nerve injury and are likely not directly involved in the repair phenotype of SCs. *Il4r* expression is upregulated in SCs in the iSNAT data, whereas this study found *Il4r* downregulated 24 h after EV stimulation, consistent with the expectation that EVs do not elicit an innate immune response upon stimulation.

As the RNA-seq analysis did not reveal sufficient differentially expressed genes with commonly used significance parameters in the comparisons of interest, expression patterns were visualized in a heatmap and analyzed by gene clustering and pathway enrichment. The heatmap revealed an upregulation in genes related to myelination at 72 h, independent of EV treatment, including the major pro-myelin transcription factor *Egr2* and *Mpz*, *Mbp*, *Pmp22*, *Mag* and *Plp1*. This is contrary to the transdifferentiation into a repair phenotype, which includes the downregulation of myelin associated genes. The slight upregulation observed here may indicate a potential shift from a repair phenotype towards remyelination. However, this upregulation is not significant and is only based on the comparison of relative expression at 24 h and 72 h. This is also contrasted by the slight increase in expression of *Gfap*, which is expected for SCs in both culture and the repair phenotype *in vivo* [13]. In the transdifferentiated state, SCs are expected to upregulate differentiation markers, such as *S100b* and *Sox10*. Here, *Sox10* exhibited relatively constant expression while *S100b* showed slight upregulation. *Ngf*, which has been demonstrated to activate autophagy in SCs and is critical in nerve regeneration [94], showed downregulation after 72 h in response to EV treatment. The macrophage attractant *Ccl2* showed upregulation after 24 h in response to EV stimulation, followed by downregulation after 72 h. This aligns with research indicating that cultured, denervated SCs secrete factors that attract macrophages [19]. However, EV stimulation did not significantly affect most expression levels. Therefore, it is not possible to draw a conclusion about their influence. The observed effects may be a result of cell confluency increasing after 96 h of culture without passage. Gene clustering and pathway enrichment revealed a gene cluster that was upregulated at 24 h and downregulated at 72 h. The genes were enriched in pathways associated with normal SC function and included ensheathment of neurons, axon ensheathment and myelination, suggesting a decline in myelinating function of the SCs. This contrasts with the upregulation seen after 72 hours in the heatmap for genes related to myelination. The information obtained from the pathway enrichment

is more comprehensive as it is based on gene clustering of the 500 most variable genes, while the heatmap only displays selected genes of interest. Additionally, a second cluster was identified with genes that were downregulated at 24 h and upregulated at 72 h. These genes were enriched in cell population proliferation, response to endogenous stimulus and cell migration. The two clusters indicate a shift from myelinating function towards proliferation and migration. However, clustering did not correlate with the EV treatment. Samples exhibited similar expression patterns at 24 h and 72 h, independent of treatment. Overall, the RNA-seq analysis did not show a readily interpretable response to EV stimulation in the data.

Recent studies have examined the impact of EV enrichment methods on their bioactivity. Some results indicate that TFF/SEC yields EVs with higher biological potency compared to UC-based methods [60, 95]. UC exposes EVs to high shear forces, which is thought to strip away loosely bound proteins on the EV surface [96]. In contrast, methods such as TFF and SEC are based on size to separate or enrich particles, which does not expose the EVs to high forces and leaves proteins bound to their surface. Size and concentration analysis of TFF/SEC-enriched EVs by NTA showed a more uniform size distribution and a larger median size at 136 nm compared to UC-enriched EVs, which had a median size of 109 nm and an irregular size distribution. The larger size of TFF/SEC EVs may be due to the presence of surface bound proteins, that have not been removed by the enrichment process. This could suggest a higher potency of EVs but would need functional testing for confirmation. This EV preparation is missing full characterization and the presence of tetraspanins would need to be demonstrated.

TFF/SEC-enriched EVs were used to stimulate SCs as a follow-up to RNA-seq, with expression of specific genes quantified by RT-qPCR. Focusing on regulators of SC repair phenotype, neuron-supportive trophic factors and proliferation markers, *Jun*, *Ngf*, *Tgfb1* and *Fgf8* were quantified. At 72 h after EV treatment, *Jun* and *Ngf* did not show increased expression. However, there was a notable range in expression levels of *Tgfb1* and *Fgf8*, with some donors exhibiting decreased expression and others showing elevated expression. These inconclusive results suggest that EVs might not have been dosed appropriately at 5,000 particles/cell for UC-enriched EVS and 20,000 particles/cell for TFF/SEC-enriched EVs. There is growing evidence that EV dosage is a critical consideration in experimental design and that dose-response curves are essential. Surprisingly, Hagey et al. recently demonstrated that the highest transcriptional responses were observed at low EV doses with high doses activating genes in lysosomal pathways, indicating EV degradation [97]. Gupta, Zickler, and El Andaloussi propose focusing on qualitative aspects of EVs rather than quantitative claims, such as stating the dose as a concentration in particles/mL [98]. This aligns with a white paper by Gimona et al., which calls for the development of potency tests as predictors of therapeutic effectiveness and

with Bremer et al., who demonstrate a functional assay with better predictiveness of function than concentration [76, 99]. Madel et al. showed an additional complication with independent EV preparations enriched from the same MSC stock exhibiting varying potency in a disease model, possibly stemming from the heterogeneity of the MSC starting material [75]. These studies highlight that the biological function of EV preparations cannot be assumed and must be assessed for each preparation individually, emphasizing the significance of EV potency over concentration measurement for dosing.

5 Conclusion and Outlook

ASC-EVs show potential to aid in nerve regeneration and for therapeutic applications. However, the mode of action of ASC-EVs remains unclear and a better understanding of EVs is needed before clinical use of EVs. This study investigated the transcriptional effects of EV stimulation but yielded inconclusive results. The lack of significant differences in gene expression cannot be solely attributed to a general lack of function of ASC-EVs. Instead, it is likely due to difficulties with dosing and potency of EVs. This study contributes to the growing body of evidence, highlighting the complexity of EV dosage and potency. If the effects of EVs are to be investigated, characterization of the EVs should include functional characterization of bioactivity and potency in addition to size, concentration and immunophenotype. There is a clear need for the development of functional assays, that are specific to EVs and Schwann cell function and are better predictors of potency than concentration alone.

Bibliography

[1] D. Grinsell and C. P. Keating. “Peripheral nerve reconstruction after injury: a review of clinical and experimental therapies.” In: *Biomed Res Int* 2014 (2014), p. 698256. DOI: 10.1155/2014/698256.

[2] E. Doron-Mandel, M. Fainzilber, and M. Terenzio. “Growth control mechanisms in neuronal regeneration.” In: *FEBS Lett* 589.14 (2015), pp. 1669–77. DOI: 10.1016/j.febslet.2015.04.046.

[3] Philippe Rigoard. *Atlas of Anatomy of the Peripheral Nerves*. 2017. ISBN: 978-3-319-43088-1. DOI: 10.1007/978-3-319-43089-8.

[4] B. L. Harty and K. R. Monk. “Unwrapping the unappreciated: recent progress in Remak Schwann cell biology.” In: *Curr Opin Neurobiol* 47 (2017), pp. 131–137. DOI: 10.1016/j.conb.2017.10.003.

[5] J. L. Salzer. “Schwann cell myelination.” In: *Cold Spring Harb Perspect Biol* 7.8 (2015), a020529. DOI: 10.1101/cshperspect.a020529.

[6] R. P. Bunge, M. B. Bunge, and M. Bates. “Movements of the Schwann cell nucleus implicate progression of the inner (axon-related) Schwann cell process during myelination.” In: *J Cell Biol* 109.1 (1989), pp. 273–84. DOI: 10.1083/jcb.109.1.273.

[7] H. J. Seddon. “Three Types of Nerve Injury.” In: *Brain* 66.4 (1943), pp. 237–288. DOI: 10.1093/brain/66.4.237.

[8] S. Sunderland. *Nerve Injuries and Their Repair: A Critical Appraisal*. Churchill Livingstone, 1991. ISBN: 9780443041617.

[9] A. Baradaran et al. “Peripheral Nerve Healing: So Near and Yet So Far.” In: *Semin Plast Surg* 35.3 (2021), pp. 204–210. DOI: 10.1055/s-0041-1731630.

[10] E. B. George, J. D. Glass, and J. W. Griffin. “Axotomy-induced axonal degeneration is mediated by calcium influx through ion-specific channels.” In: *J Neurosci* 15.10 (1995), pp. 6445–52. DOI: 10.1523/JNEUROSCI.15-10-06445.1995.

[11] E. R. Lunn, M. C. Brown, and V. H. Perry. “The pattern of axonal degeneration in the peripheral nervous system varies with different types of lesion.” In: *Neuroscience* 35.1 (1990), pp. 157–65. DOI: 10.1016/0306-4522(90)90130-v.

[12] J. Jung et al. “Actin polymerization is essential for myelin sheath fragmentation during Wallerian degeneration.” In: *J Neurosci* 31.6 (2011), pp. 2009–15. DOI: 10.1523/JNEUROSCI.4537-10.2011.

[13] T. Weiss et al. “Proteomics and transcriptomics of peripheral nerve tissue and cells unravel new aspects of the human Schwann cell repair phenotype.” In: *Glia* 64.12 (2016), pp. 2133–2153. DOI: 10.1002/glia.23045.

[14] K. R. Jessen and R. Mirsky. “The repair Schwann cell and its function in regenerating nerves.” In: *J Physiol* 594.13 (2016), pp. 3521–31. DOI: 10.1113/JP270874.

[15] C. Jopling, S. Boue, and J. C. Izpisua Belmonte. “Dedifferentiation, transdifferentiation and reprogramming: three routes to regeneration.” In: *Nat Rev Mol Cell Biol* 12.2 (2011), pp. 79–89. DOI: 10.1038/nrm3043.

[16] P. J. Arthur-Farraj et al. “c-Jun reprograms Schwann cells of injured nerves to generate a repair cell essential for regeneration.” In: *Neuron* 75.4 (2012), pp. 633–47. DOI: 10.1016/j.neuron.2012.06.021.

[17] S. Y. Jang et al. “Autophagic myelin destruction by Schwann cells during Wallerian degeneration and segmental demyelination.” In: *Glia* 64.5 (2016), pp. 730–42. DOI: 10.1002/glia.22957.

[18] J. A. Gomez-Sanchez et al. “Schwann cell autophagy, myelinophagy, initiates myelin clearance from injured nerves.” In: *J Cell Biol* 210.1 (2015), pp. 153–68. DOI: 10.1083/jcb.201503019.

[19] G. K. Tofaris et al. “Denervated Schwann cells attract macrophages by secretion of leukemia inhibitory factor (LIF) and monocyte chemoattractant protein-1 in a process regulated by interleukin-6 and LIF.” In: *J Neurosci* 22.15 (2002), pp. 6696–703. DOI: 10.1523/JNEUROSCI.22-15-06696.2002.

[20] K. R. Jessen and R. Mirsky. “The Success and Failure of the Schwann Cell Response to Nerve Injury.” In: *Front Cell Neurosci* 13 (2019), p. 33. DOI: 10.3389/fncel.2019.00033.

[21] Maximilian Haertinger. *Small extracellular vesicles derived from multipotent adipose stromal cells in peripheral nerve regeneration: jack of all trades, master of none?* presented at Small New World 2.0, Graz, Austria, Sept. 4-5, 2023.

[22] S. Y. Fu and T. Gordon. “The cellular and molecular basis of peripheral nerve regeneration.” In: *Mol Neurobiol* 14.1-2 (1997), pp. 67–116. DOI: 10.1007/BF02740621.

[23] F. Bradke, J. W. Fawcett, and M. E. Spira. “Assembly of a new growth cone after axotomy: the precursor to axon regeneration.” In: *Nat Rev Neurosci* 13.3 (2012), pp. 183–93. DOI: 10.1038/nrn3176.

[24] R. M. Stassart and A. Woodhoo. “Axo-glial interaction in the injured PNS.” In: *Dev Neurobiol* 81.5 (2021), pp. 490–506. DOI: 10.1002/dneu.22771.

[25] G. Stoll and H. W. Muller. “Nerve injury, axonal degeneration and neural regeneration: basic insights.” In: *Brain Pathol* 9.2 (1999), pp. 313–25. DOI: 10.1111/j.1750-3639.1999.tb00229.x.

[26] X. Fontana et al. “c-Jun in Schwann cells promotes axonal regeneration and motoneuron survival via paracrine signaling.” In: *J Cell Biol* 198.1 (2012), pp. 127–41. DOI: 10.1083/jcb.201205025.

[27] L. J. Wagstaff et al. “Failures of nerve regeneration caused by aging or chronic denervation are rescued by restoring Schwann cell c-Jun.” In: *Elife* 10 (2021). DOI: 10.7554/eLife.62232.

[28] K. R. Jessen and R. Mirsky. “The Role of c-Jun and Autocrine Signaling Loops in the Control of Repair Schwann Cells and Regeneration.” In: *Front Cell Neurosci* 15 (2021), p. 820216. DOI: 10.3389/fncel.2021.820216.

[29] O. A. Sulaiman and T. Gordon. “Role of chronic Schwann cell denervation in poor functional recovery after nerve injuries and experimental strategies to combat it.” In: *Neurosurgery* 65.4 Suppl (2009), A105–14. DOI: 10.1227/01.NEU.0000358537.30354.63.

[30] Gordon T Sulaiman W. “Neurobiology of peripheral nerve injury, regeneration, and functional recovery: from bench top research to bedside application.” In: *Ochsner Journal* 13.1 (2013), pp. 100–8.

[31] D. Arslantunali et al. “Peripheral nerve conduits: technology update.” In: *Med Devices (Auckl)* 7 (2014), pp. 405–24. DOI: 10.2147/MDER.S59124.

[32] F. Millesi et al. “Defining the regenerative effects of native spider silk fibers on primary Schwann cells, sensory neurons, and nerve-associated fibroblasts.” In: *FASEB J* 35.2 (2021), e21196. DOI: 10.1096/fj.202001447R.

[33] N. P. Patel, K. A. Lyon, and J. H. Huang. “An update-tissue engineered nerve grafts for the repair of peripheral nerve injuries.” In: *Neural Regen Res* 13.5 (2018), pp. 764–774. DOI: 10.4103/1673-5374.232458.

[34] X. Jiang et al. “Current applications and future perspectives of artificial nerve conduits.” In: *Exp Neurol* 223.1 (2010), pp. 86–101. DOI: 10.1016/j.expneurol.2009.09.009.

[35] S. Bolivar, X. Navarro, and E. Udina. “Schwann Cell Role in Selectivity of Nerve Regeneration.” In: *Cells* 9.9 (2020). DOI: 10.3390/cells9092131.

[36] G. Nocera and C. Jacob. “Mechanisms of Schwann cell plasticity involved in peripheral nerve repair after injury.” In: *Cell Mol Life Sci* 77.20 (2020), pp. 3977–3989. DOI: 10.1007/s00018-020-03516-9.

[37] S. V. Fazal et al. “Graded Elevation of c-Jun in Schwann Cells In Vivo: Gene Dosage Determines Effects on Development, Remyelination, Tumorigenesis, and Hypomyelination.” In: *J Neurosci* 37.50 (2017), pp. 12297–12313. DOI: 10.1523/JNEUROSCI.0986-17.2017.

[38] J. F. Stoltz et al. “Stem Cells and Regenerative Medicine: Myth or Reality of the 21th Century.” In: *Stem Cells Int* 2015 (2015), p. 734731. DOI: 10.1155/2015/734731.

[39] E. M. Horwitz et al. “Clarification of the nomenclature for MSC: The International Society for Cellular Therapy position statement.” In: *Cytotherapy* 7.5 (2005), pp. 393–5. DOI: 10.1080/14653240500319234.

[40] M. Dominici et al. “Minimal criteria for defining multipotent mesenchymal stromal cells. The International Society for Cellular Therapy position statement.” In: *Cytotherapy* 8.4 (2006), pp. 315–7. DOI: 10.1080/14653240600855905.

[41] A. Faroni, G. Terenghi, and A. J. Reid. “Adipose-derived stem cells and nerve regeneration: promises and pitfalls.” In: *Int Rev Neurobiol* 108 (2013), pp. 121–36. DOI: 10.1016/B978-0-12-410499-0.00005-8.

[42] A. J. Salgado et al. “Adipose tissue derived stem cells secretome: soluble factors and their roles in regenerative medicine.” In: *Curr Stem Cell Res Ther* 5.2 (2010), pp. 103–10. DOI: 10.2174/157488810791268564.

[43] L. Frese, P. E. Dijkman, and S. P. Hoerstrup. “Adipose Tissue-Derived Stem Cells in Regenerative Medicine.” In: *Transfus Med Hemother* 43.4 (2016), pp. 268–274. DOI: 10.1159/000448180.

[44] P. G. di Summa et al. “Adipose-derived stem cells enhance peripheral nerve regeneration.” In: *J Plast Reconstr Aesthet Surg* 63.9 (2010), pp. 1544–52. DOI: 10.1016/j.bjps.2009.09.012.

[45] F. M. Walocko et al. “The potential roles for adipose tissue in peripheral nerve regeneration.” In: *Microsurgery* 36.1 (2016), pp. 81–8. DOI: 10.1002/micr.22480.

[46] A. Musial-Wysocka, M. Kot, and M. Majka. “The Pros and Cons of Mesenchymal Stem Cell-Based Therapies.” In: *Cell Transplant* 28.7 (2019), pp. 801–812. DOI: 10.1177/0963689719837897.

[47] M. Z. Ratajczak et al. “Pivotal role of paracrine effects in stem cell therapies in regenerative medicine: can we translate stem cell-secreted paracrine factors and microvesicles into better therapeutic strategies?” In: *Leukemia* 26.6 (2012), pp. 1166–73. DOI: 10.1038/leu.2011.389.

[48] I. M. Bjorge et al. “Extracellular vesicles, exosomes and shedding vesicles in regenerative medicine - a new paradigm for tissue repair.” In: *Biomater Sci* 6.1 (2017), pp. 60–78. DOI: 10.1039/c7bm00479f.

[49] X. Liang et al. “Paracrine mechanisms of mesenchymal stem cell-based therapy: current status and perspectives.” In: *Cell Transplant* 23.9 (2014), pp. 1045–59. DOI: 10.3727/096368913X667709.

[50] S. Gurung et al. “The exosome journey: from biogenesis to uptake and intracellular signalling.” In: *Cell Commun Signal* 19.1 (2021), p. 47. DOI: 10.1186/s12964-021-00730-1.

[51] P. Wolf. “The nature and significance of platelet products in human plasma.” In: *Br J Haematol* 13.3 (1967), pp. 269–88. DOI: 10.1111/j.1365-2141.1967.tb08741.x.

[52] G. Raposo et al. “B lymphocytes secrete antigen-presenting vesicles.” In: *J Exp Med* 183.3 (1996), pp. 1161–72. DOI: 10.1084/jem.183.3.1161.

[53] R. Nieuwland et al. “Reproducibility of extracellular vesicle research.” In: *Eur J Cell Biol* 101.3 (2022), p. 151226. DOI: 10.1016/j.ejcb.2022.151226.

[54] J. P. Tosar, A. Cayota, and K. Witwer. “Exomeres and Supermeres: monolithic or diverse?” In: *J Extracell Biol* 1.6 (2022). DOI: 10.1002/jex2.45.

[55] G. van Niel, G. D’Angelo, and G. Raposo. “Shedding light on the cell biology of extracellular vesicles.” In: *Nat Rev Mol Cell Biol* 19.4 (2018), pp. 213–228. DOI: 10.1038/nrm.2017.125.

[56] C. Thery et al. “Minimal information for studies of extracellular vesicles 2018 (MISEV2018): a position statement of the International Society for Extracellular Vesicles and update of the MISEV2014 guidelines.” In: *J Extracell Vesicles* 7.1 (2018), p. 1535750. DOI: 10.1080/20013078.2018.1535750.

[57] C. C. Scott, F. Vacca, and J. Gruenberg. “Endosome maturation, transport and functions.” In: *Semin Cell Dev Biol* 31 (2014), pp. 2–10. DOI: 10.1016/j.semcdb.2014.03.034.

[58] L. Margolis and Y. Sadovsky. “The biology of extracellular vesicles: The known unknowns.” In: *PLoS Biol* 17.7 (2019), e3000363. DOI: 10.1371/journal.pbio.3000363.

[59] Maximilian Härtinger. “Novel insights into the endocytic process of adipose stem cell derived extracellular vesicles in Schwann cells.” Thesis. 2021.

[60] M. Wolf et al. “A functional corona around extracellular vesicles enhances angiogenesis, skin regeneration and immunomodulation.” In: *J Extracell Vesicles* 11.4 (2022), e12207. DOI: 10.1002/jev2.12207.

[61] E. R. Abels and X. O. Breakefield. “Introduction to Extracellular Vesicles: Biogenesis, RNA Cargo Selection, Content, Release, and Uptake.” In: *Cell Mol Neurobiol* 36.3 (2016), pp. 301–12. DOI: 10.1007/s10571-016-0366-z.

[62] Elizabeth R. Dellar et al. “Unpacking extracellular vesicles: RNA cargo loading and function.” In: *Journal of Extracellular Biology* 1.5 (2022). DOI: 10.1002/jex2.40.

[63] M. Somiya. “Where does the cargo go?: Solutions to provide experimental support for the "extracellular vesicle cargo transfer hypothesis".” In: *J Cell Commun Signal* 14.2 (2020), pp. 135–146. DOI: 10.1007/s12079-020-00552-9.

[64] B. S. Joshi et al. “Endocytosis of Extracellular Vesicles and Release of Their Cargo from Endosomes.” In: *ACS Nano* 14.4 (2020), pp. 4444–4455. DOI: 10.1021/acsnano.9b10033.

[65] S. Ghafouri-Fard et al. “The Emerging Role of Exosomes in the Treatment of Human Disorders With a Special Focus on Mesenchymal Stem Cells-Derived Exosomes.” In: *Front Cell Dev Biol* 9 (2021), p. 653296. DOI: 10.3389/fcell.2021.653296.

[66] S. Taverna, M. Pucci, and R. Alessandro. “Extracellular vesicles: small bricks for tissue repair/regeneration.” In: *Ann Transl Med* 5.4 (2017), p. 83. DOI: 10.21037/atm.2017.01.53.

[67] S. Bruno et al. “Mesenchymal stem cell-derived microvesicles protect against acute tubular injury.” In: *J Am Soc Nephrol* 20.5 (2009), pp. 1053–67. DOI: 10.1681/ASN.2008070798.

[68] M. Z. Ratajczak and J. Ratajczak. “Extracellular microvesicles/exosomes: discovery, disbelief, acceptance, and the future?” In: *Leukemia* 34.12 (2020), pp. 3126–3135. DOI: 10.1038/s41375-020-01041-z.

[69] D. Hercher, M. Q. Nguyen, and H. Dworak. “Extracellular vesicles and their role in peripheral nerve regeneration.” In: *Exp Neurol* 350 (2022), p. 113968. DOI: 10.1016/j.expneurol.2021.113968.

[70] M. A. Lopez-Verrilli et al. “Mesenchymal stem cell-derived exosomes from different sources selectively promote neuritic outgrowth.” In: *Neuroscience* 320 (2016), pp. 129–39. DOI: 10.1016/j.neuroscience.2016.01.061.

[71] M. Haertinger et al. “Adipose Stem Cell-Derived Extracellular Vesicles Induce Proliferation of Schwann Cells via Internalization.” In: *Cells* 9.1 (2020). DOI: 10.3390/cells9010163.

[72] Y. Ma et al. “Human Umbilical Cord Mesenchymal Stem Cell-Derived Extracellular Vesicles Promote the Proliferation of Schwann Cells by Regulating the PI3K/AKT Signaling Pathway via Transferring miR-21.” In: *Stem Cells Int* 2021 (2021), p. 1496101. DOI: 10.1155/2021/1496101.

[73] V. Bucan et al. “Effect of Exosomes from Rat Adipose-Derived Mesenchymal Stem Cells on Neurite Outgrowth and Sciatic Nerve Regeneration After Crush Injury.” In: *Mol Neurobiol* 56.3 (2019), pp. 1812–1824. DOI: 10.1007/s12035-018-1172-z.

[74] J. Chen et al. “Exosomes from human adipose-derived stem cells promote sciatic nerve regeneration via optimizing Schwann cell function.” In: *J Cell Physiol* 234.12 (2019), pp. 23097–23110. DOI: 10.1002/jcp.28873.

[75] R. J. Madel et al. “Independent human mesenchymal stromal cell-derived extracellular vesicle preparations differentially attenuate symptoms in an advanced murine graft-versus-host disease model.” In: *Cytotherapy* (2023). DOI: 10.1016/j.jcyt.2023.03.008.

[76] M. Gimona et al. “Critical considerations for the development of potency tests for therapeutic applications of mesenchymal stromal cell-derived small extracellular vesicles.” In: *Cytotherapy* 23.5 (2021), pp. 373–380. DOI: 10.1016/j.jcyt.2021.01.001.

[77] R. Dong et al. “MSC-Derived Exosomes-Based Therapy for Peripheral Nerve Injury: A Novel Therapeutic Strategy.” In: *Biomed Res Int* 2019 (2019), p. 6458237. DOI: 10.1155/2019/6458237.

[78] X. F. Zhao et al. “The injured sciatic nerve atlas (iSNAT), insights into the cellular and molecular basis of neural tissue degeneration and regeneration.” In: *Elife* 11 (2022). DOI: 10.7554/eLife.80881.

[79] M. E. Kastriti et al. “Schwann cell precursors represent a neural crest-like state with biased multipotency.” In: *EMBO J* (2022), e108780. DOI: 10.15252/embj.2021108780.

[80] “Bundesgesetz über Versuche an lebenden Tieren [Federal Act on Experiments on Live Animals].” In: *Bundesgesetzblatt* I Nr. 114/2012 (2012).

[81] “Directive 2010/63/EU of the European Parliament and of the Council on the protection of animals used for scientific purposes.” In: *Official Journal of the European Union* 53.L 276, 20 October 2010 (2010), pp. 33–79. DOI: 10.3000/17252555.L_2010.276.eng.

[82] T. Weiss et al. “Detailed Protocols for the Isolation, Culture, Enrichment and Immunostaining of Primary Human Schwann Cells.” In: *Methods Mol Biol* 1739 (2018), pp. 67–86. DOI: 10.1007/978-1-4939-7649-2_5.

[83] F. J. Martin et al. “Ensembl 2023.” In: *Nucleic Acids Res* 51.D1 (2023), pp. D933–D941. DOI: 10.1093/nar/gkac958.

[84] A. Dobin et al. “STAR: ultrafast universal RNA-seq aligner.” In: *Bioinformatics* 29.1 (2013), pp. 15–21. DOI: 10.1093/bioinformatics/bts635.

[85] M. I. Love, W. Huber, and S. Anders. “Moderated estimation of fold change and dispersion for RNA-seq data with DESeq2.” In: *Genome Biol* 15.12 (2014), p. 550. DOI: 10.1186/s13059-014-0550-8.

[86] B. Li and C. N. Dewey. “RSEM: accurate transcript quantification from RNA-Seq data with or without a reference genome.” In: *BMC Bioinformatics* 12 (2011), p. 323. DOI: 10.1186/1471-2105-12-323.

[87] S. X. Ge, E. W. Son, and R. Yao. “iDEP: an integrated web application for differential expression and pathway analysis of RNA-Seq data.” In: *BMC Bioinformatics* 19.1 (2018), p. 534. DOI: 10.1186/s12859-018-2486-6.

[88] J. A. Blake et al. “Mouse Genome Database (MGD): Knowledgebase for mouse-human comparative biology.” In: *Nucleic Acids Res* 49.D1 (2021), pp. D981–D987. DOI: 10.1093/nar/gkaa1083.

[89] J. R. Smith et al. “The Year of the Rat: The Rat Genome Database at 20: a multi-species knowledgebase and analysis platform.” In: *Nucleic Acids Res* 48.D1 (2020), pp. D731–D742. DOI: 10.1093/nar/gkz1041.

[90] M. Vedi et al. “2022 updates to the Rat Genome Database: a Findable, Accessible, Interoperable, and Reusable (FAIR) resource.” In: *Genetics* 224.1 (2023). DOI: 10.1093/genetics/iyad042.

[91] Martin C. Raff et al. “Galactocerebroside is a specific cell-surface antigenic marker for oligodendrocytes in culture.” In: *Nature* 274.5673 (1978), pp. 813–816. DOI: 10.1038/274813a0.

[92] K. R. Jessen et al. “Galactocerebroside is expressed by non-myelin-forming Schwann cells in situ.” In: *J Cell Biol* 101.3 (1985), pp. 1135–43. DOI: 10.1083/jcb.101.3.1135.

[93] R. Mirsky et al. “04 and A007-sulfatide antibodies bind to embryonic Schwann cells prior to the appearance of galactocerebroside; regulation of the antigen by axon-Schwann cell signals and cyclic AMP.” In: *Development* 109.1 (1990), pp. 105–16. DOI: 10.1242/dev.109.1.105.

[94] R. Li et al. “Nerve growth factor activates autophagy in Schwann cells to enhance myelin debris clearance and to expedite nerve regeneration.” In: *Theranostics* 10.4 (2020), pp. 1649–1677. DOI: 10.7150/thno.40919.

[95] R. E. Veerman et al. “Molecular evaluation of five different isolation methods for extracellular vesicles reveals different clinical applicability and subcellular origin.” In: *J Extracell Vesicles* 10.9 (2021), e12128. DOI: 10.1002/jev2.12128.

[96] M. Kokkinopoulou et al. “Visualization of the protein corona: towards a biomolecular understanding of nanoparticle-cell-interactions.” In: *Nanoscale* 9.25 (2017), pp. 8858–8870. DOI: 10.1039/c7nr02977b.

[97] D. W. Hagey et al. “The cellular response to extracellular vesicles is dependent on their cell source and dose.” In: *Sci Adv* 9.35 (2023), eadh1168. DOI: 10.1126/sciadv.adh1168.

[98] D. Gupta, A. M. Zickler, and S. El Andaloussi. “Dosing extracellular vesicles.” In: *Adv Drug Deliv Rev* 178 (2021), p. 113961. DOI: 10.1016/j.addr.2021.113961.

[99] M. Bremer et al. “Qualification of a multidonor mixed lymphocyte reaction assay for the functional characterization of immunomodulatory extracellular vesicles.” In: *Cytotherapy* (2023). DOI: 10.1016/j.jcyt.2023.03.009.

List of Figures

1 **Nerve degeneration and regeneration.** 3

2 **EV origins and signaling.** 7

3 **Characterization of SCs by flow cytometry.** 14

4 **Differentiation of ASCs into adipocytes and osteocytes demonstrates multilineage potential.** 15

5 **Characterization of UC-enriched EVs.** 16

6 **PCA plot of RNA-seq data and number of differentially expressed genes.** 17

7 **Heatmap showing expression pattern of 24 genes of interest.** 18

8 **Characterization of TFF/SEC enriched EVs by NTA.** 20

9 **Relative gene expression measured by qPCR.** 21

List of Tables

1 **Enriched pathways of 500 most variable genes.** 19

S1 **Antibodies used in flow cytometry and immunofluorescence.** 40

S2 **Primers used for qPCR.** 40

Abbreviations

AB	Antibody
AF	AlexaFluor
APC	Allophycocyanin
ASC	Adipose tissue-derived stromal cell
BSA	Bovine serum albumin
CD	Cluster of differentiation
CMG	Cell mask green
CNS	Central nervous system
CT	Cycle threshold
DAPI	4,6-diamidino-2-phenylindole
DNA	Deoxyribonucleic acid
EV	Extracellular vesicle
FC	Flow cytometry
FCS	Fetal calf serum
FDR	False discovery rate
FITC	Fluorescein isothiocyanate
FSC	Forward scatter
HBSS	Hanks balanced salt solution
HEPES	4-(2-hydroxyethyl)-1-piperazineethanesulfonic acid
IF	Immunofluorescence
ILV	Intraluminal vesicles
iSNAT	injured sciatic nerve atlas
MEM	Modified eagles medium

MSC	Mesenchymal stromal cells
MVB	Multivesicular bodies
NTA	Nanoparticle tracking analysis
P/S	Penicillin-streptomycin
PBS	Phosphate buffered saline
PCA	Principal component analysis
PE	Phycoerythrin
PFA	Paraformaldehyde
PLL	Poly-L-lysine
PNI	Peripheral nerve injury
PNS	Peripheral nervous system
QC	Quality control
RAG	Regeneration-associated gene
RNA	Ribonucleic acid
ROUT	Robust regression and outlier removal
RSC	Remak schwann cell
RT	Room temperature
RT-qPCR	Real time quantitative polymerase chain reaction
SC	Schwann cell
SCEM	Schwann cell expansion medium
SD	Standard deviation
SEC	Size exclusion chromatography
Seq	Sequencing
SSC	Side scatter

TFF Tangential flow filtration

TPM Transcripts per million

UC Ultracentrifugation

VLSI Vienna Life-Science Instruments

Appendix

Table S1: Antibodies used in flow cytometry and immunofluorescence.

Species: g : goat, h : human, m : mouse, r : rat, ha : hamster

Applications: FC : flow cytometry, IF : immunofluorescence

Antigen	Species	Host	Clone/Lot	Company	Application	Conjugate	Dilution
CD11b/c	r	h	REA325	Miltenyi	FC	PE-Vio770	1:50
CD271	h/m/r	h	REA648	Miltenyi	FC	APC	1:50
CD63	r	h	REA444	Miltenyi	FC	PE	1:1000
CD81	m/r	ha	EAT2	Miltenyi	FC	PE	1:1000
CD9	r	m	2A1/CD9	Biolegend	FC	PE	1:1000
CD90.1	m/r	h	REA838	Miltenyi	FC	FITC	1:50
Cytochrome C	h/m/r	h	REA702	Miltenyi	FC	PE	1:1000
O4	h/m/r	h	REA576	Miltenyi	FC	PE	1:50
REA CTRL	h	h	REA293	Miltenyi	FC	PE	1:1000
FABP4	h/r	g	-	RnD Systems	IF	-	1:10
Osteocalcin	h/r	m	190125	RnD Systems	IF	-	1:10
anti-goat	g	d	-	Invitrogen	IF	AlexaFluor 546	1:400
anti-mouse	m	d	-	Invitrogen	IF	AlexaFluor 488	1:400

Table S2: Primers used for qPCR.

Orientation: F : forward, R : reverse

Oligo Name	Orientation	Sequence (5' - 3')
Actb	F	GCAGGAGTACGATGAGCCG
	R	ACGCAGCTCAGTAACAGCC
Jun	F	AAACAGAAAGTCATGAACCAC
	R	CAACCAGTCAAGTTCTCAAG
Fgf8	F	GAGCAACGGCAAAGGCAAGG
	R	CTCAACTACCCGCCCTTCAC
Gapdh	F	AGTGCCAGCCTCGTCTCATA
	R	GATGGTGATGGGTTTCCCGT
Ngf	F	ATCGCTCTCCTTCACAGAGTTT
	R	TGTACGGTTCTGCCTGTACG
Tgfb1	F	CAAGCAGAGTACACACAGCA
	R	GATGCTGGGCCCTCTCCAGC